Exploring the Mechanics of Transcriptional Control through DNA Looping with Optical Tweezers

by

Yih-Fan Chen

A dissertation submitted in partial fulfillment
of the requirements for the degree of
Doctor of Philosophy
(Biomedical Engineering)
in The University of Michigan
2010

Doctoral Committee:

Associate Professor Jens-Christian D. Meiners, Chair
Associate Professor Alan J. Hunt
Associate Professor Shuichi Takayama
Associate Professor Euisik Yoon
Assistant Professor Jennifer P. Ogilvie

Dedication

This dissertation is dedicated to my parents, Wei-Zen Chen and Hsi-Chin Lee, my brother, Jyh-Jiun Chen, and Yu-Fen Hsieh for their endless support and encouragement.

Acknowledgements

I would like to express my deepest gratitude to my research advisor, Dr. Jens-Christian Meiners, for all his support and guidance throughout my PhD studies. I joined his group four years ago with limited knowledge of biophysics, but the ideal research environment in his group allows me to gradually develop the knowledge and skills needed to tackle challenging questions in biophysical research.

I would like to thank Dr. Alan Hunt, Dr. Shuichi Takayama, Dr. Euisik Yoon, and Dr. Jennifer Ogilvie for their comments and suggestions. This dissertation has been improved because of their feedback. I would also like to thank Dr. Jason Kahn for providing me with the LacI protein for my experiments.

The members of my research group have offered a great deal of help during my doctoral studies. I would particularly like to acknowledge the collaboration and friendship I have had with Josh Milstein. Without his help in experiments and modeling, many research topics presented in this dissertation would have been much more difficult. I also like to thank David Wilson for the warm welcome he offered when I first joined the group and for his continuous support and encouragement throughout my doctoral studies. Krishnan Raghunathan has also helped me a lot in my research and many other things, and I always feel very fortunate to have him as my lab mate in the past four years. I would also like to thank Gerhard Blab for providing many invaluable insights into my research and Hao Chen and Katherine Jordan for helping me in various ways. I really ap-

preciate Hao's advice on career development. Mike Chu has also helped me a lot in the preparation of DNA and cell samples, and I have been very happy to work with him.

Finally, I would like to thank my parents, Wei-Zen Chen and Hsi-Chin Lee, my brother, Jyh-Jiun Chen, and Yu-Fen Hsieh for their endless support and encouragement. Without their support, none of this would have been even possible.

The research projects presented in this dissertation were supported by The National Institutes of Health, The National Science Foundation, and funds from The University of Michigan.

Table of Contents

Dedication ..... **ii**

Acknowledgements ..... **iii**

List of Figures ..... **vii**

List of Tables ..... **xi**

List of Abbreviations ..... **xii**

Abstract ..... **xiii**

Chapter 1 Introduction **1**

1.1 Background and Motivation 1
1.2 Overview 6

Chapter 2 Stretching Submicron Biomolecules with Constant-Force Axial Optical Tweezers **8**

2.1 Introduction 8
2.2 Materials and Methods 11
2.2.1 Optical tweezers set-up 11
2.2.2 Sample preparation 14
2.2.3 Image analysis 15
2.2.4 Measuring the axial stiffness of the calibration trap 17
2.2.5 Feedback control system for drift compensation 20
2.3 Results and Discussion 21
2.3.1 Mapping the optical potential 21
2.3.2 Stretching a short DNA molecule 26
2.4 Conclusions 30

Chapter 3 Entropic Boundary Effects on the Elasticity of Short DNA Molecules **31**

3.1 Introduction 31
3.2 Materials and Methods 34
3.3 Results and Discussion 36

Chapter 4 Femtonewton Entropic Forces Can Control the Formation of Protein-Mediated DNA Loops 42

4.1 Introduction 42
4.2 Materials and Methods 44
4.3 Results and Discussion 46
4.3.1 Kinetic analysis 46
4.3.2 DNA loop topology 51

Chapter 5 Protein-Mediated DNA Loop Formation and Breakdown in a Fluctuating Environment 54

5.1 Introduction 54
5.2 Materials and Methods 56
5.3 Experimental Results 58
5.4 Modeling Results 62
5.5 Discussion 65

Chapter 6 Bead Size Effects on Protein-Mediated DNA Looping in Tethered-Particle Motion Experiments 68

6.1 Introduction 68
6.2 Materials and Methods 70
6.2.1 Tethering protocol 70
6.2.2 Imaging and analysis 71
6.3 Experimental Results 72
6.4 Discussion 74
6.4.1 Kinetic model 74
6.4.2 Entropic boundary effects 77
6.4.3 Hydrodynamic effects 79

Chapter 7 Conclusions 84

Appendix 89

Bibliography 92

List of Figures

Figure 2-1 The principle of our constant-force axial trapping scheme. A short DNA molecule is attached to a cover glass and a microsphere and placed in the linear region of the axial optical potential, which is represented by the bold curve. This holds the molecule under constant tension, irrespective of its extension. The figure shows one molecule at three different extensions, with the middle one correctly placed in the linear region, and the other two at the edges where the constant-force approximation begins to break down. 10

Figure 2-2 Schematic diagram of the optical tweezers set-up. The original laser beam is split by a polarizing beam splitter (PBS) into two beams, which are independently controlled through movable mirrors, telescopes and an acousto-optic deflector (AOD). The beams are jointly focused into the sample cell through a microscope objective. A photodetector in the back focal plane is used to measure the fluctuations of a trapped microsphere for calibration purposes. Two CCD cameras record brightfield images of the sample. One CCD camera is used to measure the axial position of the trapped microsphere, and the other is used to compensate for drift in real time. 13

Figure 2-3 Calibration of the apparent size of defocused images as a function of the axial positions of the microsphere. During the calibration, the microsphere is gradually moved toward the microscope objective by a precision piezo-stage, while video images are recorded. The size of the pattern is determined from the radial intensity distribution, as shown in the inset. The result shows that the apparent size of the image decreases linearly with the increasing distance between the microsphere and the objective. 17

Figure 2-4 Mapping the optical potential: the manipulation beam (dashed lines) and the calibration beam (solid lines) are aligned laterally, but have a different axial focus. First, a microsphere is trapped in the calibration trap of known stiffness *k*. When the manipulation beam is turned on, it exerts a small incremental force on the microsphere, which results in a displacement Δz. This displacement is measured for varying offsets between the axial foci of the two beams to map the potential of the manipulation beam as a function of axial position. 19

Figure 2-5 (*A*) Optical forces versus axial positions in the region below the laser focus. The solid lines show scaled predictions from the GLMT model. The experimental data show a constant-force region that is about 330 nm deep, where the variation in

force is less than 10%. The *x* axis shows the relative axial position with respect to the starting point of the measurement, which is about 1500 nm blow the laser focus. (*B*) Optical potentials versus axial positions in the region below the laser focus, as obtained from an integration of the optical force shown in (*A*) along the axial direction. The linear region of the optical potential is clearly discernable. 22

Figure 2-6 Optical force calibration. The optical force changes linearly with the laser intensity. The error bars show the mean ± standard error (SE) obtained from 11 independent measurements. For each measurement, 400 image frames were acquired at a frame rate of 100 fps for nine different laser intensities. The bandwidth of the measurements is limited by the thermal fluctuations of the trapped microsphere to approximately 0.1s. 24

Figure 2-7 Force-extension curve of a 1298 bp long ds-DNA molecule and a fit to the worm-like chain model. The error bars show the standard errors of means obtained from four independent measurements. In each measurement, 400 frames were taken at a frame rate of 100 fps for each force point. The entropic force resulting from the volume-exclusion effect is taken into account in the fitted curve as an offset at zero optical force. This zero-force extension of 79.9 nm corresponds to an excluded-volume force of 36.7 fN. 27

Figure 3-1 Stretching DNA with axial constant-force optical tweezers. A short DNA molecule is attached to a cover glass at one end and linked to a microsphere at the other, and a laser beam is focused into the sample cell. The tethered microsphere is placed in the linear region of the optical potential below the focal plane, where the optical force is in good approximation independent of the axial position of the microsphere. The magnitude of the optical force can be changed by varying the intensity of the laser beam. 34

Figure 3-2 Force-extension curves of four short ds-DNA constructs 1298 bp, 662 bp, 390 bp, and 247 bp in length, respectively. The lines represent fits to a modified wormlike chain model with an effective persistence length l_p^* and an excluded volume extension x_0 as adjustable parameters. The error bars represent the standard errors of means obtained from eight independent measurements. In each measurement, 400 frames were taken at a frame rate of 100 fps for each force point.. 37

Figure 3-3 The effective persistence lengths obtained by fitting a modified wormlike chain model to the four force-extension curves shown in Figure 3-2, as a function of the contour length of the molecule. For context and comparison, we also show the persistence lengths measured on longer DNA molecules by Seol *et al.*, their empirical interpolation (Eq. 3-4), and their theoretical predictions of the FWLC model of Seol *et al*. for the half-constrained boundary conditions. 39

Figure 3-4 Excluded-volume extensions and the corresponding excluded-volume forces for the four short DNA constructs shown in Figure 3-2, as a function of

contour length. The theoretical predictions for the excluded volume force calculated using Eq. 3-2 of Segall *et al*.[63] are also plotted for comparison. 40

Figure 4-1 (a) Tethered DNA is trapped in the linear region of an optical potential (dashed line indicates laser focus). The figure also represents a kinetic model of DNA looping. (b) Raw experimental recording of LacI-mediated DNA looping. The looped or unlooped threshold is chosen at the minimum between the two state distributions displayed in a histogram of the binned data. 45

Figure 4-2 Cumulative probability distributions of the observed durations that the DNA molecule remains in the looped and unlooped states under increasing force conditions (left to right). The data of (a) the looped state and (b) the unlooped state are fit to the single exponential function and a biexponential function, respectively. .. 48

Figure 4-3 Measured values for k_- (Δ), k_+ (◊), k_L (■), and k_U (◯) (see Table 4-2). The looping rate k_L is fit by the theoretical predictions for the antiparallel (solid line) and parallel (dashed line) topologies illustrated in the insert. 52

Figure 5-1 Tethered microsphere trapped in the linear region of the optical potential and stretched by fluctuating forces. Gaussian white noise with standard deviation σ is superimposed upon a set average optical force, h. 57

Figure 5-2 Experimental measurements of the (a) looped and (b) unlooped cumulative probability distributions for various noise conditions (right to left: T_α/T = 0, 0.01, 0.05, 0.12) at a mean tension of 153 fN. The data clearly show that the looped lifetimes are unaffected by the applied noise and that the unlooped lifetimes decrease with increasing noise levels. The solid lines are exponential (biexponential) fits to the looped (unlooped) data. The insert to (a) shows a typical raw trace of the DNA extension vs. time. 59

Figure 5-3 Normalized unlooped lifetimes as a function of applied noise. The (square) data points were taken at a mean tension of h = 153 fN. The (diamond) and (circle) data points were taken at h = 123 and 175 fN respectively. The three data points measured at a constant applied noise (T_α/T = 0.05) but different mean tension (h = 123, 153, 175 fN) show that the normalized lifetimes are insensitive to the average tension. The lines are the theoretical curves, shown for h = 123, 153, 175 fN, given by Eq. 5-9 with the replacement of an effective temperature $T \to T_E$. 61

Figure 5-4 The loop association process can be modeled by diffusion over a barrier. The unlooped lifetime τ_u is given by the average time it takes for the DNA to diffuse from the equilibrium position x_0, within the energy landscape, to the top of the energy barrier, of magnitude ΔU at x_1 , where it forms a looped state. 63

Figure 5-5 Unlooped lifetime τ_u as a function of a constant applied force. The solid line is the theoretical fit, given by the Kramers relation of Eq. 5-9 to the data points (squares). The coefficients of the potential $U(x; h)$ are $a = 4.64 \times 10^{-5}$ N/m and b = 739 N/m^2. 64

Figure 5-6 Schematic showing how hypothetical regulatory schemes that employ mechanical tension in DNA to control transcription can be surprisingly robust even in the presence of fluctuations. As explained in the text, since our results imply that $\tilde{k}_{t1}/k_{t1} = \tilde{k}_{t2}/k_{t2}$, a force dependent genetic switch is unaffected by the noise..... 66

Figure 6-1 Looping data for (A) Au nanoparticles and (B) polystyrene microspheres. The uppermost plots show the root mean square displacements as a function of time. The black lines result from averaging over a moving window of 2 s. The lower plots are histograms of the averaged motion showing two distinct states. 72

Figure 6-2 The data of (A) the unlooped state and (B) the looped state are fit to the biexponential function of Eq. 6-2, and the single exponential function of Eq. 6-1, respectively. For the un- looped state τ_1 = 150 ± 70 s, τ_2 = 8.6 ± 0.4 s, and c = 0.15 ± 0.03 for the Au nanoparticles and τ_1 = 80 ± 40 s, τ_2 = 10 ± 1 s, and c = 0.25 ± 0.09 s for the polystyrene microspheres. For the looped state τ = 21.5 ± 0.7 s for the Au nanoparticles and τ = 38 ± 2 s for the polystyrene microspheres. 73

Figure 6-3 Hydrodynamic surface effects on the DNA. (A) DNA tethered by a gold nanoparticle is modeled by a sphere of effective radius at a distance $b = z_{RMS}^{Au}/2$ from a planar surface. (B) DNA tethered to a large polystyrene microsphere is modeled by DNA of the same effective radius *a*, at a distance $b' = z_{RMS}^{PS}/2$ between two parallel planes. 80

List of Tables

Table 4-1 Fits to the cumulative probability distributions. 47

Table 4-2 Fits to the cumulative probability distributions. 50

Table 6-1 Rate constants from the kinetic model for gold nanoparticle and polystyrene microsphere marker beads. 77

List of Abbreviations

AOD: acousto-optic deflector

AOM: acousto-optic modulator

CCD: charge coupled device

ds-DNA: double-stranded DNA

GLMT: generalized Lorenz-Mie theory

PCR: polymerase chain reaction

TPM: tethered particle motion

WLC: worm-like chain

Abstract

The interior of a cell is a crowded and constantly fluctuating environment, where DNA and other biomolecules are highly constrained and subject to various kinds of mechanical forces. To unravel the role of mechanics in gene regulation, it is necessary to quantitatively understand the effects of mechanical tension and constraints on protein-mediated DNA looping, which is a ubiquitous theme in the regulation of the expression of prokaryotic and eukaryotic genes.

We have used the *lac* system in *Escherichia coli* as the model system to study how mechanical tension and constraints affect the formation and breakdown of regulatory protein-DNA complexes. The *lac* repressor-mediated DNA loop, which is formed when a *lac* repressor protein binds to two operator sites on a DNA molecule simultaneously, is the paradigm for protein-mediated DNA looping and is crucial to the repression of the *lac* genes.

To study the effects of mechanical constraints on the elasticity of DNA, we have developed the constant-force axial optical tweezers to manipulate submicron DNA molecules that are as short as ~250 bp in length. The force-extension curves of short DNA molecules measured using the optical tweezers show that, because of the entropic boundary effects, the persistence length of a DNA molecule is contour length-dependent and that the excluded-volume force is significant when the molecule is short. In addition, by measuring the formation and breakdown of *lac* repressor-mediated DNA loops under

static tension and fluctuating forces respectively, we have shown that the loop formation rate is sensitive to static tension on the order of only a hundred femtonewtons and to fluctuations of only a fraction of k_BT. The loop disruption rate, however, is found to be insensitive to either small static tension or small fluctuations. Moreover, our data show that the sensitivity of the loop formation rate to fluctuations is insensitive to the mean applied tension in the DNA. Our findings suggest not only that tension could be used as a means of regulating the gene transcription but that the hypothetical genetic switch can function robustly even in a noisy *in vivo* environment.

Chapter 1

Introduction

1.1 Background and Motivation

The interior of a cell is a crowded environment and a complex mechanical entity. Unlike a test tube, in which the concentration of all macromolecules is usually less than ~1-10 g/L, the interior of *Escherichia coli* (*E. coli*) cells contains ~300-400 g/L of RNA and protein[1]. The intracellular environment of eukaryotic cells is usually even more crowded because of cytoskeletal structures. In fact, macromolecules in a cell usually occupy a considerable fraction, which is typically 20-30%, of the total volume[2]. It has been known that the effects from crowding are large enough to affect the reaction rates and equilibriums significantly and to make *in vivo* and *in vitro* experimental results differ by orders of magnitude[3,4]. Moreover, since an intracellular environment is not just crowded but highly dynamic and generally not in equilibrium, many biological processes can only be described by non-equilibrium statistical mechanics rather than simple chemical reaction kinetics models. In such a crowded fluctuating intracellular environment, biological processes such as protein folding, protein assembly and protein-DNA interactions are subject to various kinds of mechanical forces and constraints, and important biomolecules usually cannot diffuse freely because of the constraints. Therefore, to obtain biologically relevant data from *in vitro* studies and to better understand the roles of mechanics in bio-

logical processes, having a quantitative understanding of the effects of mechanical forces and constraints on biological functions is required.

The mechanics of biomolecules and the response of biomolecules to mechanical forces and constraints have drawn increasing attention in the last decade[5]. Studies in mechanobiology have found mechanosensitive cells in tissues of bones, heart, blood vessels, etc. and shown that many biological reactions are sensitive to mechanical forces. Although a direct measurement of intracellular forces is still difficult nowadays, single molecule mechanical studies have shown that, for example, RNA polymerase in *E. coli* can generate forces that are more than ten piconewtons[6]. By measuring the force vs. extension curves of DNA fragments using optical tweezers, Brower-Toland *et al*. showed that it took ~15 pN to disrupt individual nucleosomes[7], and Hegner *et al*. found that the binding of RecA protein could alter the elasticity of DNA[8]. In addition, a particular class of restriction endonucleases that need to interact with DNA at two sites for efficient cleavage was found to be tension dependent and could be switched off by a force of ~1 pN[9]. The above are just a few examples of research topics relevant to biomechanics in the thriving field of single-molecule biophysics. When it comes to regulatory protein-DNA complexes, however, quantitative understanding of how their dynamics are affected by mechanical tension is still quite limited, although Normanno *et al*. have used magnetic tweezers to demonstrate that the lifetimes of the looped and unlooped states of the *lac* repressor-mediated DNA looping process could be altered by supercoiling[10].

To explore the effects of mechanical forces and constraints on the formation and breakdown of regulatory protein-DNA complexes, we have used the *lac* operon system in *E. coli* as the model system. The *lac* operon has been an important system for understand-

ing the mechanism of gene regulation since the ground-breaking work of Jacob and Monod[11]. The *lac* repressor protein (LacI) inhibits the expression of genes coding for the enzymes capable of digesting lactose when lactose is scarce in the environment of cells. A DNA loop is formed when a LacI protein binds to two *lac* operator sites simultaneously[12-15]. The formation of the LacI-mediated DNA loop is critical to the repression of *lac* genes and thus is an important part of the gene regulatory network[16]. In fact, protein-mediated DNA looping is not unique to the *lac* system but is ubiquitous in both prokaryotes and eukaryotes and is involved in the regulations of transcription, replication, and recombination[12,17,18]. For example, DNA looping is used in gene regulation in the *ara*, *deo*, *gal*, and *dln* systems along with the *lac* system in prokaryotes[17,19], and it is used to allow proteins that are far away from the genes that they control to interact with transcription factors and RNA polymerase in eukaryotes[20]. We consider that the *lac* system is a very good model system because it has been well characterized biochemically[21-23] and because the crystal structure of the lac repressor and its complexes with *lac* operator has been determined[24]. In addition, it has been studied using molecular dynamics simulations[25,26] and elastic models[27,28], and the dynamics of the LacI-DNA interactions has been measured in single molecule experiments[10,13,14,29-31].

Understanding the mechanics of protein-mediated DNA loops is the major part of this dissertation. The formation of protein-mediated DNA loops is driven by thermal fluctuations, the magnitude of which is only on the order of $k_BT/l_p = 80$ fN, where $l_p = 50$ nm is the persistence length of ds-DNA[32,33]. Since this characteristic force scale is much smaller than the typical piconewton forces present in intracellular environment, it has been predicted that the formation of protein-mediated DNA loops is very sensitive to forces

that are as small as a few hundred femtonewtons[34-36]. Therefore, although the *lac* operon system has been well understood biochemically, a quantitative understanding of its dynamics cannot be achieved if we do not understand the role of mechanics in these systems. In addition, since LacI-mediated DNA loops are crucial to the gene regulation, an even more intriguing question that has not been answered is how regulatory schemes like protein-mediated DNA looping work in the presence of intracellular forces, which are predicted to be able to affect the dynamics of protein-DNA complexes [34-36]. Therefore, although so far there has not been evidence that tension in DNA is actively regulated to control the expression of genes, we would like to first quantitatively understand the effects of tension in the substrate DNA on protein-DNA interactions.

Optical tweezers and the tethered-particle motion technique (TPM), which will be detailed later, were used in the studies presented in this dissertation to manipulate and observe a single DNA molecule each time for studying the mechanics of DNA and protein-DNA complexes. Since Arthur Ashkin and his colleagues demonstrated optical trapping in the 1970s and 1980s[37-39], optical tweezers have become important tools in biophysical studies. In addition to working as a micromanipulation tool for cells and other biomolecules, optical tweezers can be used to apply a well-calibrated force, which usually ranges between hundreds of femtonewtons to hundreds of piconewtons, to a molecule with nanometer spatial resolution. These characteristics make optical tweezers extremely useful in many biomechanical studies at the single-molecule level, in which a DNA fragment, a protein, or a protein-DNA complex is manipulated by optical tweezers to unravel the kinetics, dynamics, or mechanics of biological systems. Compared with experiments on a bulk collection of molecules, where only the averaged results but not the properties and

behavior of each individual molecule are measured, single molecule techniques such as optical trapping, single-molecule fluorescence, tethered-particle motion, etc. can give us more insights into complex biological processes. Therefore, although most of our current understanding of biology and biochemistry came from bulk experiments, single-molecule techniques have been increasingly used and have brought many intriguing findings in the last two decades. In this dissertation, for each of the optical trapping and TPM experiments presented, we observed a single DNA fragment that was attached to a cover glass at one end and to a microsphere at the other each time in. In some of the experiments, the constant-force axial optical tweezers, which will be detailed in Chapter 2, were used to trap the tethered microsphere and to apply optical forces to the DNA molecule.

The results presented in this dissertation are expected to give us an improved understanding of the mechanics that governs protein-mediated DNA looping in the highly dynamic and constrained intracellular environment. The quantitative results obtained from a series of single-molecule experiments demonstrate how DNA looping dynamics is affected by mechanical features such as tension. We believe that the effects of mechanical forces and constraints on biological functions are responsible for the discrepancy in the results of *in vivo* and *in vitro* studies of DNA looping and other biological processes. Single-molecule biomechanical studies like ours are expected to help researchers gain more biologically relevant insights from *in vitro* studies and develop models that can describe biological processes more accurately. In addition, our studies on the mechanics of DNA looping can suggest new directions for biological and biophysical research on the regulations of gene expression and other biological functions. For instance, since our results show that protein-mediated DNA looping is sensitive to tension and fluctuations (detailed

in Chapter 4 and 5), more experiments need to be done to find out whether a cell indeed actively regulates tension to control the transcription of genes or has a mechanism that can compensate for the effects of mechanical forces. Overall, our results suggest that effects of mechanical forces and constraints on biological functions are significant. These effects need to be further studied quantitatively using experimental approaches other than traditional biochemical and biological techniques so that we can better understand the role of mechanics in biological systems.

1.2 Overview

This dissertation is organized as follows. Chapter 2 shows the design of and the calibration procedures for the constant-force axial optical tweezers, which are capable of manipulating DNA molecules shorter than what can be manipulated by conventional optical tweezers. In Chapter 3, the contour length-dependent elasticity of submicron DNA molecules and the excluded-volume forces measured using the constant-force axial optical tweezers are presented. Chapter 4 shows the dramatic effects of femtonewton forces on the formation and breakdown of protein-mediated DNA loops, which are crucial to the regulation of gene transcription. The determination of the loop topology from the measurements of the force sensitivity of DNA loops is also discussed. Chapter 5 demonstrates the effects of fluctuating forces on the dynamics of DNA looping and explains why tension could be a robust means of regulating gene transcription even in a noisy *in vivo* environment. A fluctuating barrier model for the loop formation process in a noisy environment is also detailed. In Chapter 6, the lifetimes of the looped and unlooped states measured with both 800 nm polystyrene microspheres and 50 nm gold nanoparticles are presented to show the bead size effects on DNA looping in tethered-particle motion experi-

ments. Chapter 7 summarizes the major findings of all the studies described in this dissertation.

Chapter 2

Stretching Submicron Biomolecules with Constant-Force Axial Optical Tweezers

Optical tweezers have become powerful tools to manipulate biomolecular systems, but are increasingly difficult to use when the size of the molecules is < 1 μm. Many important biological structures and processes, however, occur on the sub-micron length scale. Therefore, we have developed and characterized an optical manipulation protocol that makes this length scale accessible by stretching the molecule in the axial direction of the laser beam, thus avoiding limiting artifacts from steric hindrances from the microscope cover glass and other surface effects. The molecule is held under constant mechanical tension by a combination of optical gradient forces and back-scattering forces, eliminating the need for electronic feedback. We demonstrate the utility of this method through a measurement of the force-extension relationship of a 1298 bp ds-DNA molecule.

2.1 Introduction

Optical tweezers have become an important tool to study the mechanics of biomolecules and biomolecular processes. In a typical experiment, the molecule or molecular system of interest is attached on one end to a microsphere, which serves as a handle of opti-

cal manipulation, and on the other end either to a second microsphere or, more often, to a solid support such as a microscope cover glass. A laser beam is then used to move the microsphere in the focal plane of the objective, thus applying a force to the molecule. These techniques serve well when it comes to the manipulation of molecules that are several microns in length, but become increasingly difficult when sub-micron sized systems are to be studied.

The ability to manipulate shorter molecules reliably is important, however, because molecules that extend freely for microns are scarce in living cells. DNA, for instance, is subject to a number of constraints, which range from packing by histones into chromatin in eukaryotes to attachments to the cytoskeleton and cell wall in prokaryotes. In order to get closer to this highly constrained in-vivo situation, techniques that can look at shorter DNA fragments are required. Another reason why working with shorter molecules is advantageous is that amplitude of the thermal fluctuations of the molecule held under constant tension scales linearly with its length[40]. Thus, reducing the length of the molecule makes events of interest, such as stepping of a molecular motor or binding of a protein easier to observe. Similar considerations have also been applied to magnetic tweezers, and in one study, a reduction of molecular length from 4 kb to 2 kb resulted in a twofold improvement in the signal/noise ratio[41].

The reason why stretching shorter molecules with optical tweezers is technically difficult is mostly related to the fact that when the molecule is attached to the cover glass on one end, the angle between the extended molecule and the cover glass becomes steeper as the molecule gets shorter. This means that the microsphere sees an anisotropic optical potential in which the trap gets softer as the force is no longer applied purely in the focal

plane, but increasingly in the axial direction. Thus applying a well-calibrated force during the stretching protocol is almost impossible. Furthermore, the microspheres used as handles are rarely perfectly round, and tend to preferentially align themselves in the anisotropic optical potential and rotate somewhat when pulled. This in turn makes accurate displacement measurements problematic. To overcome these problems, we present a scheme in which the microsphere is no longer moved in the focal plane of the microscope and the molecule is always stretched perpendicular to the cover glass in the axial direction (see Figure 2-1). This geometry is reminiscent of magnetic tweezers, but without the complication of uncontrolled torques from having a magnetic center of the microsphere that often does not coincide with the geometric center, which is primarily limiting how short the molecules in magnetic tweezers can be.

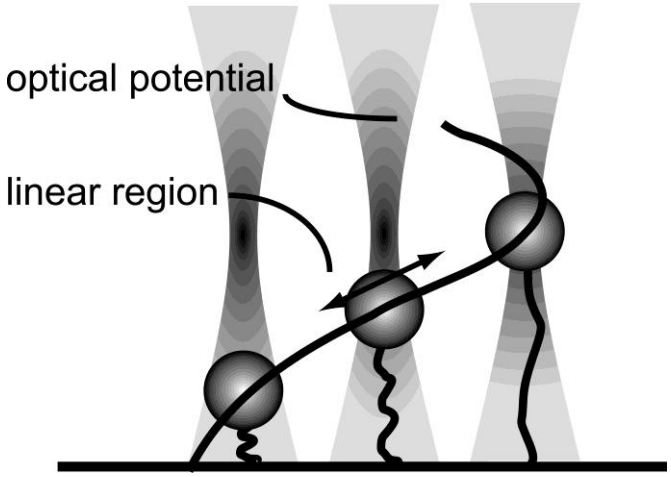

Figure 2-1 The principle of our constant-force axial trapping scheme. A short DNA molecule is attached to a cover glass and a microsphere and placed in the linear region of the axial optical potential, which is represented by the bold curve. This holds the molecule under constant tension, irrespective of its extension. The figure shows one molecule at three different extensions, with the middle one correctly placed in the linear region, and the other two at the edges where the constant-force approximation begins to break down.

Another important consideration for our scheme is the need to hold the molecule under constant tension, no matter what its extension is, which is required by many experimental protocols. Typical examples are the motion of molecular motors where the DNA is reeled in[42,43] or the observation of protein binding and unbinding events where the apparent length of the DNA depends on the binding state[7]. Conventionally in optical trapping, the microsphere is held in the parabolic minimum of the optical potential, resulting in an applied force proportional to the displacement of the microsphere from the center of the trap. To obtain a constant force instead, electronic feedback is generally employed. More recently passive schemes in which linearly shaped optical potentials are used for the purpose of applying a constant force irrespectively of the extension of the system have been introduced[44,45]. Similarly, Greenleaf *et al*.[46] used the approximately linear region of an optical potential from a Gaussian beam to locally create constant-force conditions. The elimination of the feedback led to an increased bandwidth and decreased measurement noise, enabling them to see motion with single base pair resolution[47]. We apply the same principle to axial optical manipulation and trap the microsphere in the linear region of the combined optical potential from the Gaussian intensity gradient and the backscattering force (Figure 2-1).

2.2 Materials and Methods

2.2.1 Optical tweezers set-up

The optical set-up of the constant-force axial optical tweezers shown in Figure 2-2is very similar to conventional dual beam optical tweezers such as the one described by Meiners and Quake.[48] A linearly polarized beam from a 1064-nm Nd:YVO_4 laser (T40-

Z-106C, Spectra-Physics, Mountain View, CA) is split into two orthogonally polarized beams of variable intensity. One of these beams is eventually used to manipulate the biomolecule of interest, and the other serves calibration purposes. In the following, they will be referred to as manipulation beam and calibration beam, respectively. To control the intensity of the manipulation beam independently and avoid interference effects between the beams, a computer-controlled acousto-optic deflector (AOD, DTD-274HA6, IntraAction, Bellwood, IL) is inserted into the manipulation beam path. Beamsteering mirrors control independently the direction of both beams; and separate telescopes on motorized translation stages allow us to focus the beams into different focal planes, with differing beam sizes, if desired. After the beams are recombined on a second polarizing beam splitter, a final telescope conditions the beam parameters before an oil immersion microscope objective with a high numerical aperture (PlanApo 60X/1.40 oil, Olympus, Center Valley, PA) focuses the beams into the sample cell. To obtain optimal trapping efficiency with the calibration beam, its beam parameters are chosen such that it overfills the back aperture of the microscope objective 1.5-fold, whereas an overfill factor of 1.2 for manipulation beam gave us a somewhat shallower focus and therefore a larger constant-force region in the optical potential to work with.

The optical tweezers are integrated into a custom-built brightfield microscope. The sample is mounted on a precision piezo-stage (Nano-LP100, Mad City Labs, Madison, WI) that controls the position of the sample with respect to the objective. A condenser and a halogen lamp are used to provide illumination from the other side of the microscope objective. The brightfield image is separated from the laser trapping beam paths through a dichroic mirror, and imaged on two CCD cameras. The digital CCD camera

(PL-A741, PixeLINK, Ottawa, Canada) is our main means of data acquisition, and triggered under computer control to take brightfield videos or images of the sample at a desired sampling rate synchronized with any manipulation protocol. In addition, a secondary CCD camera (WAT-902B, Watec, Orangeburg, NY) is used as a part of a feedback control system that compensates for thermal and mechanical drifts in the microscope. It enables virtually unlimited observation time by automatically adjusting the stage such that a reference microsphere that is stuck to the cover glass always remains in the same position and focus.

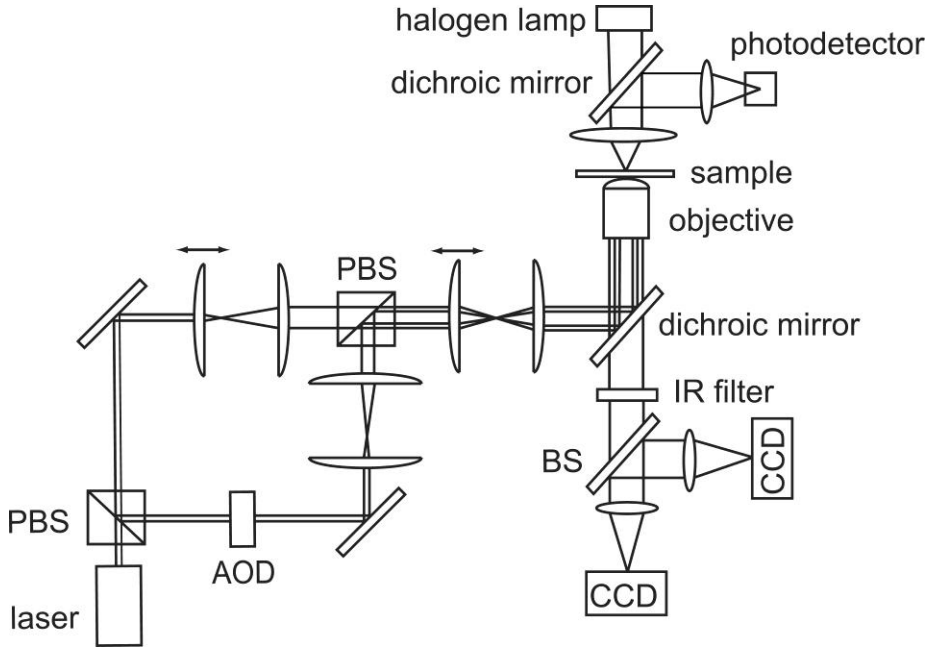

Figure 2-2 Schematic diagram of the optical tweezers set-up. The original laser beam is split by a polarizing beam splitter (PBS) into two beams, which are independently controlled through movable mirrors, telescopes and an acousto-optic deflector (AOD). The beams are jointly focused into the sample cell through a microscope objective. A photodetector in the back focal plane is used to measure the fluctuations of a trapped microsphere for calibration purposes. Two CCD cameras record brightfield images of the sample. One CCD camera is used to measure the axial position of the trapped microsphere, and the other is used to compensate for drift in real time.

In addition, we collect the transmitted and forward-scattered laser light with the illumination condenser and project it onto a photodetector (ET-3020, Electro-Optics Technology, Traverse City, MI) such that the laser spot overfills the active area of the photodetector approximately 1.2-fold. This allows a measurement of the displacement of a trapped microsphere in the axial direction from fluctuations in the intensity of this signal, as the spot size at the detector changes with the position of the microsphere[49,50]. The signal from the photodetector is filtered by an anti-aliasing filter with a cutoff frequency of 100 kHz and amplified by a low-noise amplifier (SR560, Stanford Research Systems, Sunnyvale, CA) before it is acquired by a data acquisition card (PCI-6025E, National Instruments, Austin, TX) at a sampling rate of 200 kHz.

2.2.2 Sample preparation

DNA molecules of interest are attached to the cover glass on one end and to a microsphere on the other end using digoxigenin-antibody and biotin-streptavidin chemistry following protocols that are similar to those used in other tethered-particle and optical tweezers experiments[13,29]. For our experiments, we used a ds-DNA fragment with a length of 1298 bp. It is obtained by PCR from the pRW490 plasmid of Hsieh *et al.*[51], using primers with biotin and digoxigenin modifications on the 5' end.

The sample chamber for tethered particle experiments consists of a microscope slide, a cover glass, and a parafilm spacer in between. First, two access holes are drilled into a microscope slide, Tygon tubing is inserted, and affixed with epoxy glue. Then the parafilm spacer with a cutout for the flow channel between the holes and the cover glass are

sandwiched together and baked to create a sealed chamber with a volume of about 9 μl. in the center of the slide.

To attach the DNA and microspheres, the chamber is first filled with a solution containing 20 μg/ml anti-digoxigenin (anti-digoxigenin from sheep, Roche, Indianapolis, IN) in PBS (137 mM NaCl, 10 mM Phosphate, 2.7 mM KCl, pH 7.4) and left to incubate for 20 minutes at room temperature. Then, the excess anti-digoxigenin is washed away by 200 μl of PTC buffer (20 mM Tris–Acetate, pH 8.0, 130 mM KCl, 4 mM $MgCl_2$, 0.1 mM EDTA, 0.1 mM DTT, 20 μg/ml BSA, 80 μg/ml Heparin). To prevent non-specific binding, the chamber is washed again with 200 μl of PTC1 buffer (PTC buffer plus 1 mg/ml α-casein) and left to incubate for half an hour. Separately, a 30 μl volume of a DNA-microsphere mixture that contains 1 ng/ml of end-labeled DNA and 60 pM of streptavidin-coated polystyrene microspheres (800 nm in diameter, Spherotech, Lake Forest, IL) in PTC1 buffer is spun slowly on a rotating rack at room temperature for half an hour to allow microspheres to bind to DNA molecules without sedimentation. Then, the DNA-microsphere mixture is introduced into the prepared chamber and incubated for 5 minutes. Finally, the camber is flushed with 500 μl of PTC1 buffer to remove any unbound DNA and microspheres. By using an excess of microspheres we assure that virtually each of the remaining tethered microspheres is bound to a single DNA molecule. Before using the sample, the inlet and outlet tubes of the chamber are sealed to prevent evaporation and fluid flow.

2.2.3 Image analysis

In the constant-force axial optical tweezers set-up, the position of a trapped microsphere is measured by analyzing the size of its defocused brightfield image as captured

by the CCD camera using procedures similar to those described by Revyakin *et al*. for magnetic tweezers[52]. To measure the apparent sizes of the images, the geometric pattern matching function in LabVIEW is utilized to find the center of the image of the microsphere first. Then, a radial intensity profile is obtained by averaging cross sections of the image over 360° around the center. Then the peak of the radial profile, which corresponds to the white ring in the brightfield images in Figure 2-3, is fit with a quadratic function, and the distance between this maximum and the center of the image is used as a measure for the apparent size of the image of the microsphere. To obtain a calibration curve, a microsphere that is stuck to the cover glass is initially placed about 1 μm below the focus of the microscope objective in order to obtain a clear defocused image. Then, this distance is gradually increased using the calibrated piezoelectric microscope stage while additional images are acquired. From the analysis of these images, we construct the calibration curve that yields the apparent sizes of the images as a function of the axial positions of the microsphere, as shown in Figure 2-3. The statistical error for each data point is 0.0045 pixels or 1.35 nm, as determined from the scatter between measurements in successive video frames. Despite this low noise, multiple calibration runs under nominally identical conditions resulted in a variation of the slopes of the measured microsphere sizes versus axial positions of as much as 5%. We attribute this systematic uncertainty in our calibration primarily to mechanical drifts in the system. These drifts cannot be compensated by the autofocus feedback control system detailed below because the drift-induced change in the apparent sizes of the stuck microsphere cannot be measured correctly when the piezostage is moved axially during the calibration. In fact, the feedback control system has to be disabled temporarily to avoid interfering with the calibration. Nevertheless, since the

calibration of the microsphere size versus axial position can be accomplished in less than one minute, the effect of the slow drifts is not significant.

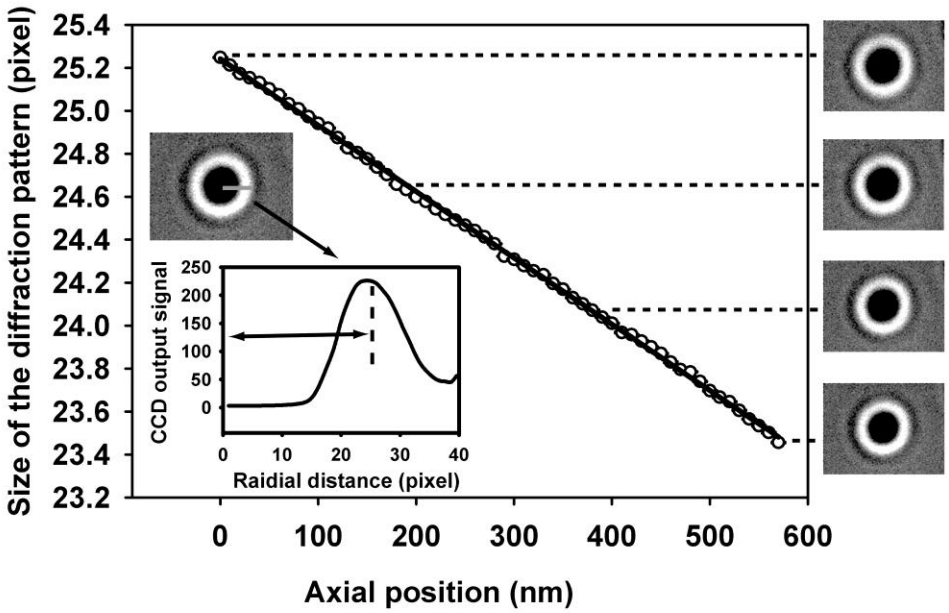

Figure 2-3 Calibration of the apparent size of defocused images as a function of the axial positions of the microsphere. During the calibration, the microsphere is gradually moved toward the microscope objective by a precision piezo-stage, while video images are recorded. The size of the pattern is determined from the radial intensity distribution, as shown in the inset. The result shows that the apparent size of the image decreases linearly with the increasing distance between the microsphere and the objective.

2.2.4 Measuring the axial stiffness of the calibration trap

The purpose of measuring the axial stiffness of the calibration trap is to calibrate the optical force in the linear region of the optical potential created by the manipulation beam. Therefore, we measure the optical potential of the manipulation beam first to identify the axial position of the linear region, which will be detailed later. After the optical potential of the manipulation beam is mapped, the calibration trap is moved to the same height as the linear region of the manipulation beam by moving the telescope lenses, as shown in

Figure 2-4. Then, the axial stiffness of the calibration trap is measured while the manipulation beam is turned off. For this purpose, a free microsphere is trapped in the calibration trap, whose focus was located 0.98 μm above the cover glass. At this distance, electrostatic interactions with the surface can safely be disregarded, as the Debye screening length under our buffer conditions is approximately 0.8 nm. The photodetector for the transmitted laser light is used to record the thermal motion of the microsphere in the axial direction. The autocorrelation of this signal is then computed and then fit with a single exponential decay function to obtain the time constant τ_z of the fluctuations[48,53-55]. For a typical laser intensity of 48 mW at the back aperture of the microscope objective, we found a time constant of 4.62 ± 0.09 ms. From this time constant and the friction coefficient of the microsphere ζ, the stiffness of the calibration trap is found as $k_z = \zeta / \tau_z$. The hydrodynamic friction coefficient of the microsphere is corrected for the proximity of the surface using the expansion by Brenner[56] and Neuman and Block[57]:

$$\varsigma = 6\pi\eta r \frac{4}{3}\sinh\alpha \sum_{n=1}^{\infty} \frac{n(n+1)}{(2n-1)(2n+3)} \times \left[\frac{2\sinh(2n+1)\alpha + (2n+1)\sinh 2\alpha}{4\sinh^2(n+1/2)\alpha - (2n+1)^2 \sinh^2\alpha} - 1 \right], \qquad (2\text{-}1)$$

where

$$\alpha = \cosh^{-1}\left(\frac{h}{r}\right) = \ln\left\{\frac{h}{r} + \left[\left(\frac{h}{r}\right)^2 - 1\right]^{1/2}\right\},$$

ζ is the friction coefficient, r is the radius of the microsphere, h is the height of the center of the microsphere above a surface, η is the viscosity of the fluid, and $6\pi\eta r$ is the Stokes drag coefficient. Ten terms of Eq. 2-1 are used to obtain the friction coefficient ζ, given that the sum in Eq. 2-1 converges quite quickly.

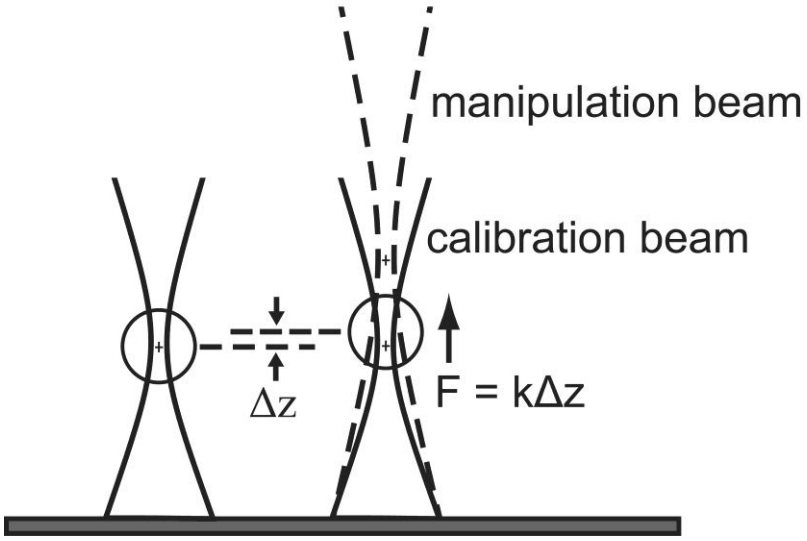

Figure 2-4 Mapping the optical potential: the manipulation beam (dashed lines) and the calibration beam (solid lines) are aligned laterally, but have a different axial focus. First, a microsphere is trapped in the calibration trap of known stiffness *k*. When the manipulation beam is turned on, it exerts a small incremental force on the microsphere, which results in a displacement Δz. This displacement is measured for varying offsets between the axial foci of the two beams to map the potential of the manipulation beam as a function of axial position.

Under our experimental conditions, Eq. 2-1 represents a 77.5% correction to the Stokes drag coefficient in free solution, yielding a final value of 1.2×10^{-8} kg/s for the drag coefficient when the proximity of the surface is taken into account. The stiffness of the calibration trap is then 2.59 pN/μm. The most important uncertainty in this calibration is the aforementioned systematic error in the determination of the axial position of the microsphere, because the correction to the Stokes drag coefficient is not insignificant. The estimated 5% error in the measurement of the axial position results in an error of ~4% in the calibration of the optical trap stiffness. An additional source of error stems from the temperature dependency of the viscosity of the buffer, which contributes an additional 1-2% to the overall calibration error. Overall, we estimate that we have an error of approximately 6% in the calibration of the axial stiffness of the trap. It is worth noting

that, when the height of the microsphere h is smaller, the friction coefficient ζ and thus the calculated stiffness k_z, are more sensitive to the change in h because the hydrodynamic proximity of the surface becomes more significant. In other words, it is more accurate to measure the stiffness with the microsphere at a higher position from the cover glass because the measurement is less sensitive to errors in the measurement of the trap height. On the other hand, any stiffness calibration should be made close to where the actual measurement takes place. Otherwise, changes in trap stiffness as a function of distance from the cover glass[50] dominate the overall error. The result of the trade-off in accuracy is that we calibrate the trap stiffness of the calibration beam and map the optical potential of the manipulation beam 800-1000 nm above the cover glass, which is ~300 nm higher than the position where tethered DNA molecules are manipulated.

2.2.5 Feedback control system for drift compensation

Like any microscope, our set-up is subject to thermal and mechanical drifts that place time limits on precision measurements. In order to compensate for these drifts we employ an autofocus feedback mechanism. In addition to the trapped object, we observe another microsphere that is laterally close to the optical trap but stuck to the cover glass by a secondary camera at a frame rate of 30 fps. Axial movement of the stuck microsphere with respect to the focal plane of the objective also reflects the drift experienced by a trapped microsphere with respect to the cover glass. Therefore, we continuously analyze the images captured by the secondary camera with a custom LabVEW program in real time to determine the changes in the apparent sizes of the images, which correspond to the drifts in the axial direction. Based on the magnitude and the direction of the drift, a proportional-integral (PI) control loop generates an output voltage on the data acquisition card (PCI-

6025E, National Instruments, Austin, TX), which in turn controls the position of the piezo-stage to cancel the drift. Therefore, the time of optical trapping is almost unlimited by drifts.

2.3 Results and Discussion

The demonstration and characterization of the constant-force optical tweezers consists of two parts: First, we carefully map the optical potential of the manipulation beam with the help of the calibration trap. Second, we use the manipulation beam to stretch and hold a 1298 bp DNA fragment under constant tension.

2.3.1 Mapping the optical potential

In order to map the optical potential of the manipulation beam and calibrate the optical forces that it exerts, we trap a free microsphere in the calibration trap. Then the collinearly aligned manipulation beam is turned on, which exerts an additional optical force on the trapped microsphere[55] (see Figure 2-4). It is worth noting that for such a calibration measurement the calibration trap needs to be substantially stronger than the manipulation beam. Typically, we used 48 mW at the back aperture of the objective for the calibration beam and intensities of up to 9 mW for the manipulation beam. The axial displacement of the microsphere in the calibration trap that results from the force exerted by the manipulation beam is measured by video analysis from the defocused brightfield image as described above. It was under all circumstances less than 170 nm and well within the range of our calibration.

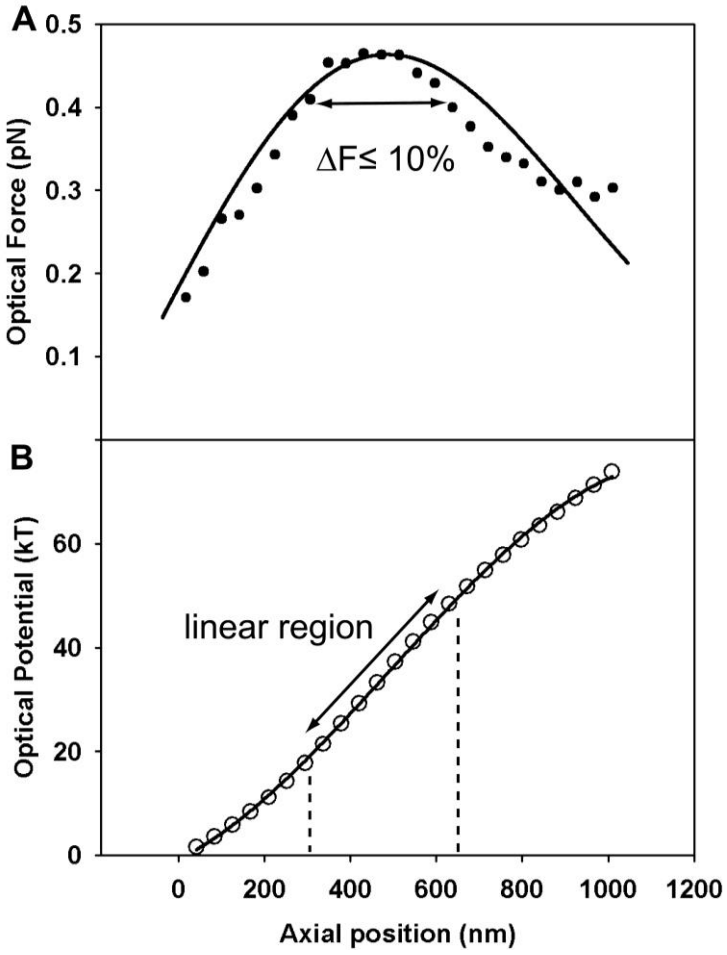

Figure 2-5 (*A*) Optical forces versus axial positions in the region below the laser focus. The solid lines show scaled predictions from the GLMT model. The experimental data show a constant-force region that is about 330 nm deep, where the variation in force is less than 10%. The *x* axis shows the relative axial position with respect to the starting point of the measurement, which is about 1500 nm blow the laser focus. (*B*) Optical potentials versus axial positions in the region below the laser focus, as obtained from an integration of the optical force shown in (*A*) along the axial direction. The linear region of the optical potential is clearly discernable.

To map the optical potential along the axis of the manipulation beam, we moved one of the telescope lenses such that the focus of the calibration beam moves axially. Since the calibration beam is much stronger than the manipulation beam, the trapped microsphere mostly moved with the axial movement of the calibration beam focus, while the manipulation beam adds a small incremental displacement that is proportional to the ma-

nipulation force of interest, as shown in Figure 2-4. This incremental displacement is determined as a function of axial position from a differential measurement of the microsphere position in the presence and absence of the manipulation beam. The center of the linear region of the manipulation beam was then determined as the position where the displacement was largest. We then moved the calibration trap to the same height as the linear region and measured the stiffness of the calibration trap using the autocorrelation method described above. Using this calibration, we obtain the optical force of the manipulation beam as a function of the axial position as shown in Figure 2-5 *A.* This yields the profile of the optical potential of the manipulation beam along the axial direction as shown in Figure 2-5 *B* through integration.

The linear region of the optical potential is clearly discernable. If we define the constant-force region as the region over which the force varies by less than 10%, we can determine that the constant-force region extends for 330 nm in the axial direction. As expected, this constant-force region is longer than what Greenleaf *et al*. reported on their lateral optical trap[46], given that the intensity distribution of a Gaussian beam is shallower in the axial direction than in the lateral direction. These results suggest that the linear region allows us to stretch a DNA molecule with an approximately constant force as long as the length of the DNA molecule changes by ~1000 basepairs or less. Given that the change in DNA length upon protein binding is usually smaller, this region is long enough to study the effect of force on the interactions between proteins and DNA. In addition, this useful operating range dovetails nicely with where conventional optical micromanipulation become unusable in the sub-micron range and allows the study the mechanical properties of shorter biomolecules.

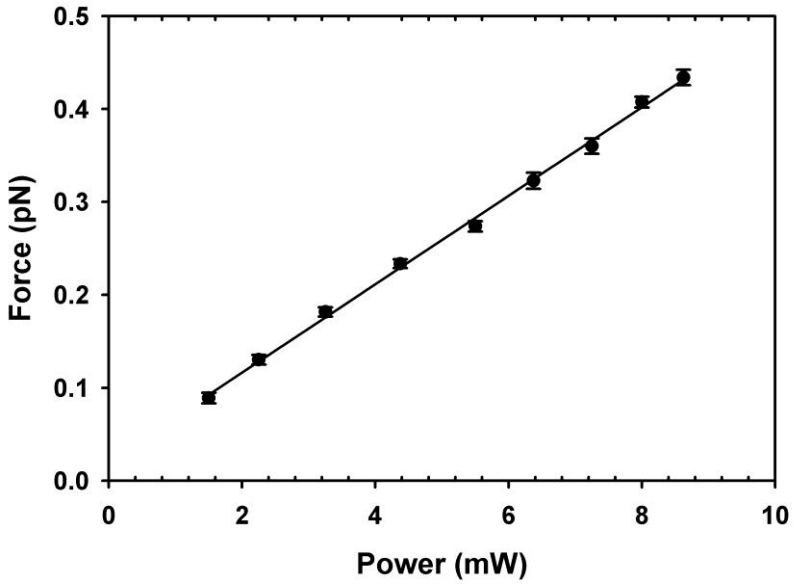

Figure 2-6 Optical force calibration. The optical force changes linearly with the laser intensity. The error bars show the mean ± standard error (SE) obtained from 11 independent measurements. For each measurement, 400 image frames were acquired at a frame rate of 100 fps for nine different laser intensities. The bandwidth of the measurements is limited by the thermal fluctuations of the trapped microsphere to approximately 0.1s.

During the course of these experiments, we noted that the exact location of the linear region changes slightly when the distance between the microscope objective and the cover glass is changed (data not shown). Specifically, we found that the linear region moves closer to the objective when the distance between the cover glass and the objective is shorter. This is consistent with the reports by Deufel and Wang[50] and Neuman *et al.*[58], who reported that the laser focus moves closer to the microscope objective when the cover glass is moved towards the objective. The change in the optical potential is due to the spherical aberrations caused by the refractive index mismatch between the cover glass and the buffer solution in the chamber.

After the optical potential of the manipulation beam was characterized, we established the relationship between laser power in the manipulation beam and optical force in the linear region, as this is how a varying desired force is applied in biomolecular stretching applications. For this purpose, we positioned the trapped microsphere at the center of the linear region of the optical potential. We then measured the displacements of the microsphere as a function of laser intensity, yielding the desired force calibration, as shown in Figure 2-6. The observed linear relationship between laser power and optical force also confirms that the microsphere was indeed placed in the linear region of the optical potential.

Under these experimental conditions, we estimate that the absolute measurement of the optical force is accurate to within 10%, as systematic errors arise mostly from the measurement of the axial positions and the calibration of the axial stiffness. We note, however, that relative measurements, such as comparisons of the elasticity of two different DNA molecules, can be accomplished with considerably higher accuracy because of the outstanding linearity of the power – force relationship in Figure 2-6, as long as the microsphere remains within the linear region of the optical potential. If, on the other hand, the microsphere leaves this linear region due to errors in the initial alignment or exceedingly large changes of the extension of the molecule, errors in excess of the 10% calibration error may result.

To quantitatively model our experiment, we used the generalized Lorenz-Mie theory (GLMT) to solve the Maxwell's equations for scattering by particles of arbitrary size[59,60]. The force acting on the particle in the axial direction using GLMT is given by[59,60]

$$F_Z = \frac{n_m}{c} I_m C_{pr,z} = \frac{n_m}{c} \frac{2P}{\pi \varpi_0^2} C_{pr,z}, \tag{2-2}$$

where

$$C_{pr,z} = \frac{\lambda^2}{2\pi} \sum_{n=1}^{\infty} \left\{ \begin{array}{l} \frac{2n+1}{n(n+1)} |g_n|^2 \, \mathrm{Re}\left(a_n + b_n - 2a_n b_n^*\right) \\ + \frac{n(n+2)}{n+1} \mathrm{Re}\left[g_n g_{n+1}^* \left(a_n + b_n + a_{n+1}^* + b_{n+1}^* - 2a_n a_{n+1}^* - 2b_n b_{n+1}^*\right)\right] \end{array} \right\}.$$

I_m is the intensity at the focus, n_m is the refractive index of the medium, c is the speed of light in vacuum, P is the beam power, ω_0 is the beam waist, $C_{pr,z}$ is the cross section for radiation pressure, a_n and b_n are Mie coefficients, which are functions of the size and the refractive index of the microsphere, and g_n are beam-shape coefficients. To solve Eq. 2-2, we used the Optical Tweezers Computational Toolbox of Nieminen *et al.*[61], using P = 0.25mW, refractive indices of n_m = 1.33 and n_p = 1.59 for the medium and the particle, and an effective numerical aperture of 1.4. Qualitatively, the results agree with our experiments and show the approximately linear region of the optical potential that we are using for optical force-clamping. Because of uncertainties in some of our parameters, such as the infrared transmission of the microscope objective and the actual laser beam profile, the results of the GLMT calculation were linearly scaled by a factor of 4.0 to fit the experimental data. These fitted force and potential curves are shown together with the experimental data in Figure 2-5.

2.3.2 Stretching a short DNA molecule

With the force calibration in hand, we measure the force-extension relationship of a 1298 bp long ds-DNA, as shown in Figure 2-7, following in the footsteps of similar expe-

riments for longer molecules with contour lengths of 32.8 μm[32], 1.3 μm[33] and 0.6 μm[62]. For this purpose, we positioned the manipulation beam above a DNA-tethered microsphere such that the microsphere is at the beginning of the linear region of the potential when the DNA is not extended by an external force.

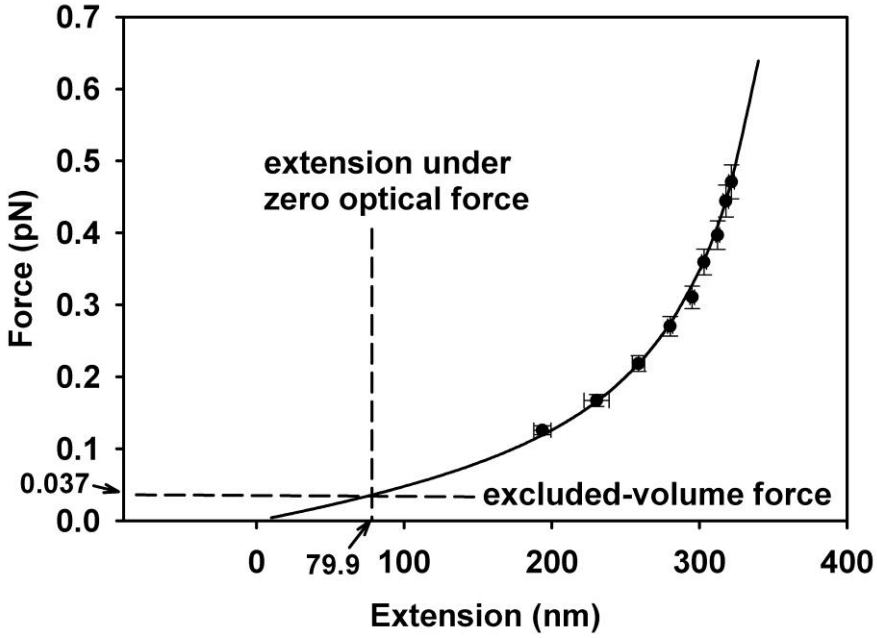

Figure 2-7 Force-extension curve of a 1298 bp long ds-DNA molecule and a fit to the worm-like chain model. The error bars show the standard errors of means obtained from four independent measurements. In each measurement, 400 frames were taken at a frame rate of 100 fps for each force point. The entropic force resulting from the volume-exclusion effect is taken into account in the fitted curve as an offset at zero optical force. This zero-force extension of 79.9 nm corresponds to an excluded-volume force of 36.7 fN.

To assure ourselves that we were indeed in the correct position, we adjusted the axial position of the cover glass with respect to the objective first and then adjust the axial position of the focus of the manipulation beam using one of the motorized telescopes until the DNA molecule is within the linear region, which is apparent when the extension of the DNA is least sensitive to the motion of the telescope. With this alignment in place, we

determined the relationship between the optical force and the extension of the DNA molecule by varying the intensity of the manipulation beam.

It is important to note that the average extension of the DNA in the absence of any external optical force is not zero. This residual entropic stretching force results from volume-exclusion effects due to the proximity of the DNA and the tethered microsphere to the cover glass, which they cannot penetrate. A theoretical and computational analysis by Segall *et al.*[63] show that the volume-exclusion effect between the tethered microsphere and the cover glass becomes more significant with increasing excursion number $N_R \equiv R / (Ll_p/3)^{1/2}$, which is a function of the radius R of the microsphere, the contour length L of the DNA molecule, and its persistence length l_p. They suggest that under the Gaussian-chain approximation the effective force resulting from excursions can be estimated by

$$\left\langle F_{eff} \right\rangle = \frac{k_b T}{\pi^{1/2}\left(L l_p/3\right)^{1/2}}\left(\frac{1-e^{-N_R^2}}{erf\,(N_R)}\right), \tag{2-3}$$

Since this excluded-volume force is difficult to measure directly with sufficient accuracy, we incorporate the corresponding excluded-volume extension x_0 as an adjustable parameter into fits of the data to the worm-like chain (WLC) model as approximated by Marko and Siggia[64] for an extended polymer. The total force acting on the DNA is thus

$$F_{opt} + F_{WLC}(x_0, l_p, L) = F_{WLC}(x_0 + x_{opt}, l_p, L), \tag{2-4}$$

where F_{opt} is the optical force exerted by the manipulation beam, x_0 is the extension under zero optical force, x_{opt} is the incremental extension of the molecule under optical force. $F_{WLC}(x, l_p, L)$ is the force of an extended polymer in the worm-like chain model,

$$F_{WLC} = \left(\frac{k_B T}{l_p}\right)\left[\frac{1}{4(1-x/L)^2} - \frac{1}{4} + \frac{x}{L}\right]. \tag{2-5}$$

Using the crystallographic axial rise of ds-DNA of 0.34 nm per base pair, we fixed the contour length of our DNA at 441 nm. Leaving the persistence length and the excluded-volume extension as adjustable parameters, we found l_p = 33.9 nm and x_0 = 79.9. The extension of 79.9 nm corresponds to an excluded-volume force of 36.7 fN, compared to 33 fN estimated by Eq. 2-3. In addition, the persistence length of 33.9 nm is significantly smaller than generally accepted values around 50 nm, as determined in several single molecule experiments[33,64-66].

Fits to an improved worm-like chain model proposed by Bouchiat *et al.*[66] did not appear to improve the accuracy or change the results of our measurements significantly, because the added higher-order terms decreased the numerical stability of the fitting algorithm significantly. According to Bouchiat *et al.*, the persistence length obtained from the fit to Marko and Siggia's WLC model typically overestimates the persistence length by at most ~5% for our range of extensions. Given that the uncertainty in our calibration is roughly 10%, the error in the persistence length due to the Marko-Siggia approximation is comparatively small.

Seol *et al.*[62] provide a different explanation for the discrepancy in the persistence length from the literature value. They suggest that when the elasticity of ds-DNA is analyzed within the framework of the WLC model, the effective value for the persistence length is not fully independent of the contour length of the molecule. In fact, they report a reduction of more than 10% in the persistence length for a molecule with a contour length of less than 1.3 μm. More specifically, the persistence lengths of their 864-nm, 756-nm, 666-nm, and 632-nm DNA molecules, which are their four shortest DNA molecules, are 44 nm, 43 nm, 42.4 nm, and 42.1 nm respectively, as estimated from figure 9 of Ref.[62].

They attributed the decrease of the effective persistence length with the contour length of DNA to the lack of considerations of finite chain length, chain-end boundary conditions, and the microsphere rotational fluctuations inherent in optical trapping assays. To describe this finite-length effect, they suggest scaling the persistence length as

$$l_p = \frac{l_{p\infty}}{1 + a l_{p\infty} / L}, \tag{2-6}$$

with $l_{p\infty}$ = 51.51 nm and an empirical parameter a = 2.78. For our molecule with a contour length L of 441 nm, which is shorter than those use by Seol *et al*., Eq. 2-6 yields an effective persistence length of 38.8 nm, which is close to our experimental result of 33.9 nm, considering that we have a systematic error of about 5% in the measurement of molecular extensions.

2.4 Conclusions

We have demonstrated and characterized a novel protocol for applying optical tweezers to manipulate sub-micron biomolecules. The attached microsphere is pulled away from the cover glass, reducing unwanted artifacts from steric hindrances and other surface effects. The use of a combination of optical gradient forces and back-scattering forces allows the application of a constant optical force that is independent of the extension of the molecule.

We have applied this method to measure the force-extension relationship of a 1298 bp ds-DNA molecule, and found that its elastic behavior is well-described by the wormlike chain model by Marko and Siggia[64] when excluded-volume effects from the proximity of the cover glass are taken into account and the persistence length is corrected for finite-length effects as proposed by Seol *et al*.[62].

Chapter 3

Entropic Boundary Effects on the Elasticity of Short DNA Molecules

We have measured the entropic elasticity of double-stranded-DNA molecules ranging from 247 to 1298 bp in length using axial force-clamp optical tweezers. We show that entropic end effects and excluded-volume forces from surface attachments become significant for such short molecules. The effective persistence length of the shortest molecules decreases by a factor of two compared to the established value for long molecules, and excluded-volume forces extend the molecules to about one third of their nominal contour length. We interpret these results in the framework of an inextensible semiflexible rod model.

3.1 Introduction

Entropic springs are an important manifestation of thermally fluctuating mechanical systems and are relevant for understanding a wide range of phenomena that range from the structure of biopolymers to rubber elasticity[64,67]. Long double-stranded (ds)-DNA molecules have become the paradigm for entropic springs ever since Smith *et al.*[32] measured the elasticity of a single 32.8-μm-long ds-DNA molecule using magnetic tweezers.

Their data were described well by the wormlike chain (WLC) model of Marko and Siggia[64]. The WLC model gives the entropic force of an inextensible polymer as

$$F_{WLC} = \left(\frac{k_B T}{l_p}\right)\left[\frac{1}{4(1-\varepsilon)^2} - \frac{1}{4} + \varepsilon\right], \tag{3-1}$$

where l_p is the persistence length of the polymer and $\varepsilon = x/L$ is the relative extension of the molecule x with respect to its contour length L. It is important to note that the force depends only on the relative extension, but not on the absolute length of the molecule. The persistence length, then, is a measure of intrinsic entropic elasticity of the polymer in a fashion similar to the reciprocal of Young's modulus of a classical elastic material. In a polymer, however, the modes of thermal fluctuations that are supported by the molecule depend on the boundary conditions for the end as well as other constraints that may have been placed on it, such as excluded volumes. Therefore, in very short molecules, where modes that involve the ends contribute significantly[68], or in heavily constrained systems, the notion of an intrinsic entropic elasticity as described by a universal persistence length breaks down. This effect has been observed in stiff microtubules where the contour length is much shorter than the persistence length[69]. We believe that this also explains the significant decrease in the effective persistence length of the sub-micron DNA molecules of ~50 % that we report in this study. Evidence for such an effect in DNA in a regime where the contour length is comparable or longer than the persistence length has come from two kinds of experiments. First, ring cyclization experiments with very short (~100 bp) ds-DNA fragments showed that the cyclization rates of the DNA are often significantly higher than expected[70], which points to enhanced flexibility. Some inconsistencies in these results, though, remain. They have been mainly attributed to the intricacies of the

hybridization and ligation process[71], but it has also been suggested that the exact boundary conditions for the hybridization step, i.e. how much angular alignment of the overhanging ends is required, affect this particular process as well. This in turn may lead to the apparently contradictory results when an effective persistence length of the DNA is calculated from these experiments[72]. Second, a measurement of the elasticity of a surface-tethered 1870-bp-long ds-DNA molecule with an attached micron-sized polystyrene microsphere by Seol *et al.*[62] using optical tweezers yielded a persistence length of 42 nm, which is ~16% less than the commonly accepted value of ~50 nm for long molecules under these ionic conditions. Seol *et al.* attribute most of this effect to boundary conditions imposed on the system by the surface and the microsphere, but cannot rule out actual changes in the intrinsic bendability of the molecule on short length scales. While the geometric constraints in the tethered-particle motion experiments may seem highly artificial, they are unbiological only in the sense that transcriptionally active DNA is free to fluctuate only over hundreds of base pairs, not thousands. The attachments to surfaces and microspheres may mimic, for instance, attachment to adjacent histones. Excluded-volume constraints, from an impenetrable surface in the tethered-microsphere geometry, have been analyzed theoretically by Segall *et al.*[63] who predicted that the associated excluded-volume forces become increasingly stronger as the length of the molecules decreases. Under our experimental conditions, these forces are mostly associated with the impenetrability of the cover glass to the microsphere and less attributable to the exclusion of the DNA from these volumes. While the excluded-volume forces have been observed in measurements of the distribution of the tethered microsphere positions[73], they have not been studied quantitatively. In fact, most analyses of tethered-particle experiments that

use this geometry have conveniently ignored them altogether[74], even though the induced stretch can substantially affect processes such as protein-DNA complex formation, which is often studied in this kind of experiment[13]. In this study, we present measurements of the elasticity and excluded-volume forces of surface-tethered ds-DNA fragments that range from 247 to 1298 bp in length and show that the effective persistence length for the shortest of these molecules drops to as little as 28 nm while excluded-volume effects stretch it to 34% of its nominal contour length.

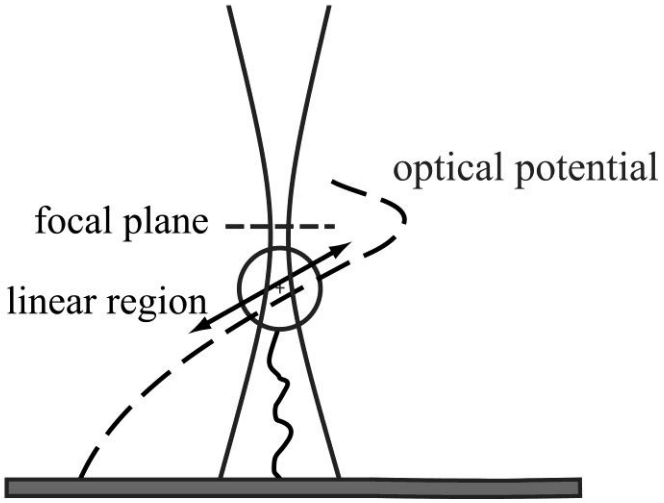

Figure 3-1 Stretching DNA with axial constant-force optical tweezers. A short DNA molecule is attached to a cover glass at one end and linked to a microsphere at the other, and a laser beam is focused into the sample cell. The tethered microsphere is placed in the linear region of the optical potential below the focal plane, where the optical force is in good approximation independent of the axial position of the microsphere. The magnitude of the optical force can be changed by varying the intensity of the laser beam.

3.2 Materials and Methods

Experimentally, we measured the force-extension relationships of four short ds-DNA fragments, which are 1298, 662, 390, and 247 bp in length, using axial optical force-clamp tweezers. The molecules were attached with one end to the bottom of a flow cell

using digoxigenin-antibody binding and with the other end to a polystyrene microsphere with a diameter of 800 nm using biotin-streptavidin binding. Each of the functional groups is attached to one strand of the DNA backbone through a six-carbon linker. This essentially makes each attachment point a swivel joint that can pivot in all directions. Details of the sample preparation and characterization protocol are described by Chen *et al.*[75].

The force-extension relationship for the DNA molecules is measured by applying an optical force to the microsphere and then measuring the corresponding extension of the molecule. For this aim, the microsphere is placed in the approximately linear region of the axial optical potential, extending the DNA perpendicularly away from the cover glass, as shown in Figure 3-1. The optical force that acts on the microsphere is then a combination of the gradient and the scattering forces, which remains constant to within 10% over a range of 330 nm. The details of the experimental set-up, the characterization, and the calibration process for the optical potential are described by Chen *et al.*[75]. This axial optical force-clamp geometry has distinct advantages over conventional in-plane optical tweezers when the goal is to study the mechanics of sub-micron biomolecules in a quantitatively accurate fashion. The principal complication with in-plane stretching is that the angle between the DNA and the axis of the optical tweezers changes as the molecule is extended. This in turn may lead to a rotation of the microsphere. Since the microspheres are generally not perfectly spherical, measurement errors in the molecular extension result, which can be substantial when they are compared to the very small dimensions of the molecule itself. The axial geometry employed here does not suffer from these problems.

In order to obtain accurate elasticity measurements, we need to take entropic stretching forces that result from excluded-volume effects in the tethered-particle geometry properly into account. According to the theoretical and the computational analyses by Segall *et al.*, the motion of a microsphere of radius *R* in a tethered particle experiment is increasingly constrained as the excursion number, $N_R \equiv R \Big/ \left(L l_p / 3 \right)^{1/2}$, rises. By modeling the tethered DNA fragment as a Gaussian chain, Segall *et al.* estimated the effective force resulting from the impenetrability of the cover class to the microsphere as

$$F_{eff} = \frac{k_B T}{\pi^{1/2} \left(L l_p / 3 \right)^{1/2}} \left(\frac{1 - e^{-N_R^2}}{erf\left(N_R \right)} \right). \tag{3-2}$$

3.3 Results and Discussion

To take the volume exclusion effects into account in our data analysis, we fit our data of the measurements of the force-extension relationships to a modified wormlike chain model, which incorporates the excluded-volume extension x_0 as an adjustable parameter in the fits and subsumes boundary-condition effects into an effective persistence length l_p^*. The excluded-volume force, which is calculated using the WLC model with the extension x_0 and the effective persistence length l_p^* instead of l_p, is added to the curve fitting equation to reflect the fact that the DNA molecule is stretched by both the optical and the excluded-volume forces. The modified fit equation is

$$F_{opt} = F_{WLC}\left(x_0 + x_{opt}, l_p^*, L \right) - F_{WLC}\left(x_0, l_p^*, L \right), \tag{3-3}$$

where F_{WLC} is the WLC model, as given by Eq. 3-1; F_{opt} is the optical force exerted by the laser beam, which is obtained from the calibration of the optical tweezers; x_0 is the

extension under zero optical force; x_{opt} is the extension resulting from the optical force; and $F_{WLC}\left(x, l_p^*, L\right)$ is the force of an extended polymer in the wormlike chain model. In the measurement of the force-extension relationships, we applied optical forces of different magnitudes F_{opt} and measured the corresponding extensions x_{opt}. Then, we fitted the data to Eq. 3-3 to obtain x_0 and l_p^*. As shown in Figure 3-2, this model describes the experimental data well.

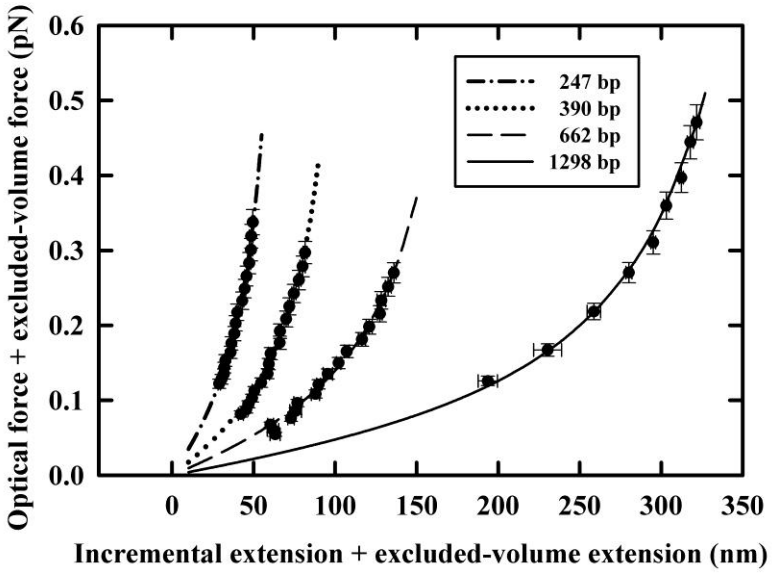

Figure 3-2 Force-extension curves of four short ds-DNA constructs 1298 bp, 662 bp, 390 bp, and 247 bp in length, respectively. The lines represent fits to a modified wormlike chain model with an effective persistence length l_p^* and an excluded volume extension x_0 as adjustable parameters. The error bars represent the standard errors of means obtained from eight independent measurements. In each measurement, 400 frames were taken at a frame rate of 100 fps for each force point.

Our main finding is that the effective persistence length drops dramatically as the contour length of the molecule decreases, as shown in Figure 3-3, down to 27.9 nm for the 247 bp construct. This result is consistent with measurements of the elasticity of

much longer DNA fragments ranging from 1870 to 7138 bp by Seol *et al.*[63], even though their analysis used a solution to the WLC model that does not include the excluded volume effects between the microsphere and the cover glass. To compare our measurements to their data, we used their empirical interpolative formula,

$$l_p^* = \left(\frac{l_{p\infty} T}{1 + a l_{p\infty} / L} \right) \tag{3-4}$$

with $l_{p\infty} = 51.51\,\text{nm}$ and a fitted empirical parameter $a = 2.78$[62]. We note that the effective persistence lengths obtained from our measurements follow this interpolation formula well, even though we extend the range of the measurements by almost an order of magnitude. We can further compare our data to the finite wormlike chain model by Seol *et al.*, which incorporates corrections for the finite chain length, the chain-end boundary conditions, and the microsphere rotational fluctuations. For our experimental geometry, half-constrained boundary conditions in which the tangent vector of the DNA at both ends is free to explore half of the orientational space in a hemispherical fashion are chosen. The reduced effective persistence length in this model is due to the additional freedom of the end tangent vector, which is more constrained when the DNA fragment is part of a longer chain. As shown in Figure 3-3, this model predicts our observed effective persistence lengths quite well, without any adjustable or empirical parameters. The small discrepancy for our longest DNA construct can likely be attributed to deviations of the optical potential from a perfectly linear shape for large extensions.

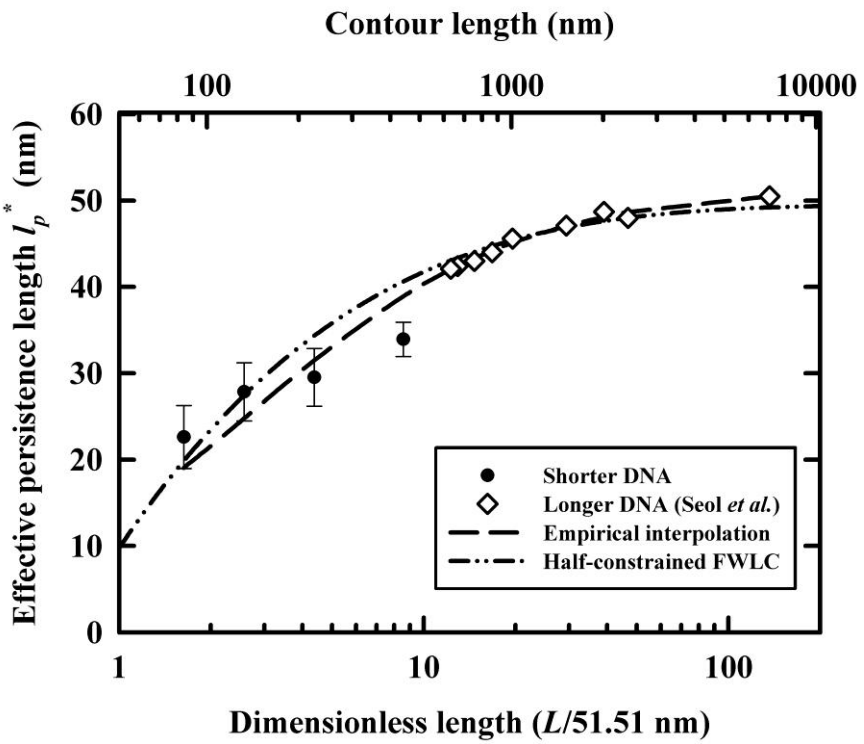

Figure 3-3 The effective persistence lengths obtained by fitting a modified wormlike chain model to the four force-extension curves shown in Figure 3-2, as a function of the contour length of the molecule. For context and comparison, we also show the persistence lengths measured on longer DNA molecules by Seol *et al*., their empirical interpolation (Eq. 3-4), and their theoretical predictions of the FWLC model of Seol *et al*. for the half-constrained boundary conditions.

The other result from our measurements is the determination of the excluded-volume forces from the impenetrability of the cover glass to the microsphere. The corresponding forces and extensions of the DNA molecules are shown in Figure 3-4. Comparing the excluded-volume forces to the values calculated using Eq. 3-2 from Segall *et al.*[63] with the measured effective persistence length l_p^*, we note a good agreement. This shows that the effective repulsive force from the interactions between the microsphere and the cover glass can be significant, and stretch the DNA to as much as a third of its nominal contour length. This is particularly important for tethered-particle experiments, as forces that are

comparable to the characteristic force scale of entropic forces in ds-DNA, $k_B T / l_{p\infty} = 80$ fN, are thought to have a significant impact on the assembly of regulatory protein-DNA[35,36], which is commonly probed in this kind of experiments[13].

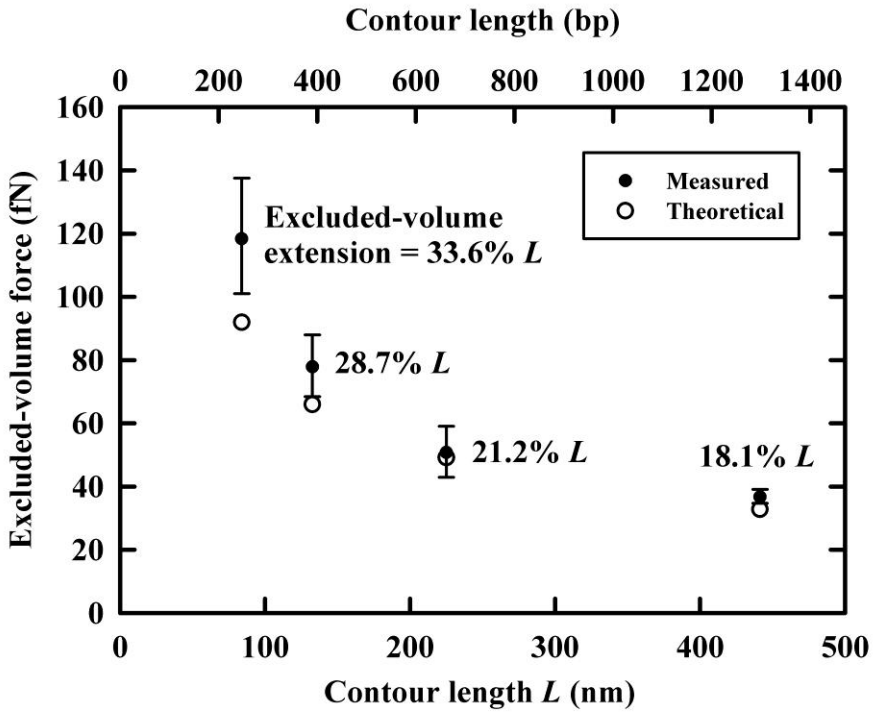

Figure 3-4 Excluded-volume extensions and the corresponding excluded-volume forces for the four short DNA constructs shown in Figure 3-2, as a function of contour length. The theoretical predictions for the excluded volume force calculated using Eq. 3-2 of Segall *et al*.[63] are also plotted for comparison.

In conclusion, we have measured the effective persistence length and the excluded-volume extension of surface-tethered sub-micron DNA molecules using constant force axial optical tweezers. Because of the special geometry of this optical tweezing scheme, accurate measurements of the elasticity of short DNA molecules have become feasible, allowing us to manipulate molecules that are almost an order of magnitude shorter than

what can be studied with conventional optical tweezers. The measurements reveal a significant reduction in the effective persistence length of the ds-DNA constructs with a decreasing contour length. We attribute this observation to entropic boundary effects that allow the orientation of the ends to explore a significant conformational space, and not changes in the intrinsic bendability of the molecules. The effective persistence length as a function of contour length is well described by the empirical interpolation by Seol *et al* [62] and agrees with the theoretical predictions of the half-constrained FWLC model. The effect is quite dramatic: the effective persistence length of the 247 bp-long DNA molecule drops to nearly half of the established value for long DNA molecules. Thus, we conclude that when the WLC model by Marko and Siggia[64] is used to model the elasticity of very short DNA fragments in models for chromatin, for instance, or to interpret the experimental data in tethered-particle experiments with sub-micron DNA molecules, an effective persistence length that is appropriate for the boundary conditions in a given geometry can and should be used.

Moreover, we have shown that the excluded-volume constraints from the impenetrable surface in the tethered-microsphere geometry can result in significant entropic stretching forces when DNA molecules are short. We see a good quantitative agreement with the predictions by Segall *et al*.[63], which suggest that the excluded-volume effects for such short DNA molecules are dominated by volume exclusion effects between the microsphere and the cover glass. These effects can indeed be crucial for interpreting tethered-particle experiments, as the associated excluded-volume force can easily become larger than the characteristic force scale for entropic forces in ds-DNA, $f_c = k_B T / l_{p\infty} = 80$ fN.

Chapter 4

Femtonewton Entropic Forces Can Control the Formation of Protein-Mediated DNA Loops

We show that minuscule entropic forces, on the order of 100 fN, can prevent the formation of DNA loops—a ubiquitous means of regulating the expression of genes. We observe a tenfold decrease in the rate of LacI-mediated DNA loop formation when a tension of 200 fN is applied to the substrate DNA, biasing the thermal fluctuations that drive loop formation and breakdown events. Conversely, once looped, the protein-DNA complex is insensitive to applied force. Our measurements are in excellent agreement with a simple polymer model of loop formation in DNA, and show that an antiparallel topology is the preferred LacI-DNA loop conformation for a generic loop-forming construct.

4.1 Introduction

Since the ground-breaking work of Jacob and Monod on gene regulations, the lac operon has become a canonical example of how prokaryotic cells regulate the expression of genes in response to changes in environmental conditions[11,15,76]. The lac operon is responsible for the efficient metabolism of lactose in *E. coli* bacteria ensuring that enzymes capable of digesting lactose are produced only when needed. The lac repressor-mediated

DNA loop, which is formed when tetrameric lac repressor protein binds to two lac operator sites simultaneously, is an important part of this gene regulatory network and is crucial for the repression of lac genes[16,77]. Long range genetic regulation by DNA looping, however, is not unique to the lac operon, but appears in a variety of contexts within prokaryotes, such as the *ara* or *gal* operons, and is ubiquitous within eukaryotes[12]. While the biochemistry of these processes is generally well understood, the mechanics of the assembly and breakdown of protein-mediated DNA loops has only recently garnered much attention[13,29,78]. In this study, we investigate the role that tension in the substrate DNA plays in the formation and breakdown of protein-mediated DNA loops, and conclude that loop formation is acutely sensitive to entropic forces on the hundred-femtonewton scale.

Protein-mediated DNA loop formation is driven by thermal fluctuations in the DNA which bring distant operators close enough for loop closure by a protein. However, it is quite surprising that the magnitude of these fluctuations, which one can estimate as $k_B T/l_p \approx 80\ \text{fN}$, where $l_p = 50\ \text{nm}$ is the persistence length, is much smaller than the typical piconewton forces that arise in the intracellular environment, from molecular motors or DNA-cytoskeletal attachments, for example. This observation has led to predictions that forces as small as a few hundred femtonewtons are sufficient to reduce the loop formation rate by more than two orders of magnitude[35,36,64,79]. Given that the cellular environment is thought to regularly subject protein-DNA complexes to large static or fluctuating forces, the cell must either use mechanical pathways to regulate genetic function, or compensate for the effects of tension to ensure the stable control of gene expression.

4.2 Materials and Methods

To experimentally study the effects of tension on the kinetics of DNA looping, we used optical tweezers in conjunction with tethered-particle motion (TPM) measurements to investigate the formation and breakdown of LacI-mediated DNA loops under a constant stretching force. We report three main results: First, the rate of loop formation is extremely sensitive to applied tension resulting in a tenfold decrease in loop formation when increasing the tension from 60 to 183 fN. Second, the lifetime of the looped state appears to be completely unaffected by forces as large as 183 fN. Third, our measurements strongly suggest that the antiparallel conformation is the dominant topology of a generic LacI-mediated DNA loop[80]. We mechanically attenuate the thermal fluctuations that drive loop formation and breakdown, and measure the associated changes to the looping and unlooping rates, by employing a variety of optical tweezers that differ from the more conventional tweezers setup. Constant-force axial optical tweezers stretch the molecule away from the surface and trap the attached microsphere slightly below the laser focus in an approximately linear region of the optical potential. This provides effectively a constant force in the axial direction that does not change when the protein binds to or dissociates from the DNA [see Figure 4-1(a)]. Details of this setup are described in Ref. [75]. Because of this novel optical tweezers setup, we have been able to measure the formation and breakdown rates of LacI-mediated loops as a function of applied tensile force in the femtonewton range.

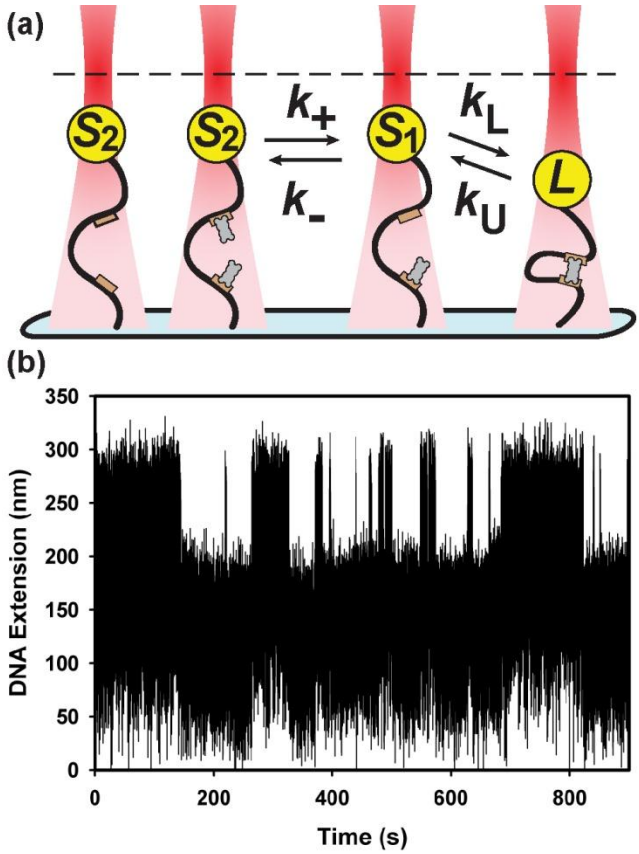

Figure 4-1 (a) Tethered DNA is trapped in the linear region of an optical potential (dashed line indicates laser focus). The figure also represents a kinetic model of DNA looping. (b) Raw experimental recording of LacI-mediated DNA looping. The looped or unlooped threshold is chosen at the minimum between the two state distributions displayed in a histogram of the binned data.

The DNA samples used in this study were prepared in a similar way to that of other TPM experiments[75]. We surface-tethered a 1316-bp ds-DNA molecule with two symmetric lac operators spaced 305 bp apart and then attached an 800 nm polystyrene microsphere to the other end, which was trapped within the linear regime of the optical potential. The total tension in the DNA was carefully calibrated to account for the applied optical force[75] and volume exclusion effects arising from entropic interactions between the microsphere and the cover glass[81]. The looping and unlooping lifetimes were measured under four different forces: 60(±5), 78(±6), 121(±9), and 183 (±15) fN in the presence of

100 pM of LacI protein. In each measurement, the surface-tethered ds-DNA molecule was stretched by a constant force while the CCD camera captured defocused images of the tethered microsphere at a frame rate of 100 fps. The looped and unlooped states of the DNA molecule, which correspond to different axial positions of the microsphere, can be measured by analyzing the resulting images, as shown in Figure 4-1(b). By directly observing changes in the axial position of the microsphere, the temporal resolution for detecting loop formation and breakdown events in our experiment is as low as 300 ms, an order of magnitude better than conventional TPM. However, as we decrease the applied tension, it becomes increasingly difficult to resolve changes in the size of the microsphere, and at zero optical force, we must resort to conventional TPM. Moreover, even in the absence of an optical force, a residual entropic force from excluded volume effects remains. For this reason, we were not able to obtain a direct measure of the force free loop formation and breakdown rates.

4.3 Results and Discussion

4.3.1 Kinetic analysis

The data was analyzed by first extracting the elapsed times between loop formation and breakdown events from time traces like the one in Figure 4-1(b). Then, for each force condition, the lifetime of each state was determined from a fit to the cumulative probability distribution, as shown in Figure 4-2. The resulting distribution displayed by the looped state is well fit by a single exponential function

$$P(t:\tau) = 1 - e^{-t/\tau}, \tag{4-1}$$

with time constant τ. However, the data of the unlooped state is poorly fit to a single exponential function, but is well fit to a biexponential function

$$P_2(t:\tau_1,\tau_2) = cP(t:\tau_1) + (1-c)P(t:\tau_2), \tag{4-2}$$

with time constants τ_1 and τ_2, and dimensionless fitting parameter c. Results of the fits are shown in Table 4-1.

Table 4-1 Fits to the cumulative probability distributions.

Force (fN)	60 ± 5	78 ± 6	121 ± 9	183 ± 15
Looped				
τ(s)	20 ± 0.3	22.5 ± 0.2	24.1 ± 0.3	24.8 ± 0.7
Unlooped				
τ_1(s)	3.0 ± 0.2	4.0 ± 0.42	9.7 ± 0.4	14.5 ± 1
τ_2(s)	31 ± 8	54 ± 10	91 ± 10	101 ± 6
c	0.77 ± 0.03	0.77 ± 0.02	0.74 ± 0.02	0.38 ± 0.03

One of the most striking features of the data in Figure 4-2 is that the dissociation time constant of DNA loops is unaffected by increasing the force from 60 to 183 fN. This result is in contrast to the force dependence of the time necessary to form a loop, which increases significantly with only a modest increase in applied tension. To interpret these observations quantitatively, we begin by applying a kinetic model for the underlying processes of protein binding, unbinding, loop formation, and breakdown, as illustrated in Figure 4-1(a). This is the simplest model of the kinetics that is both consistent with our data and what is currently known about LacI-mediated looping.

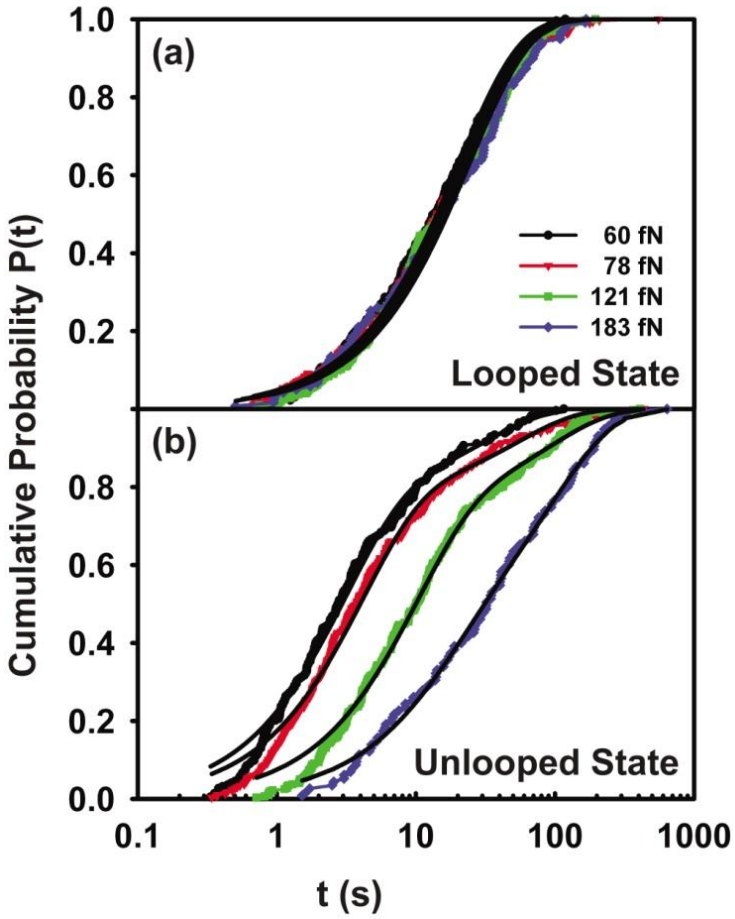

Figure 4-2 Cumulative probability distributions of the observed durations that the DNA molecule remains in the looped and unlooped states under increasing force conditions (left to right). The data of (a) the looped state and (b) the unlooped state are fit to the single exponential function and a biexponential function, respectively.

If we collect all time intervals that start at a loop formation event (L) and end at a loop breakdown event (S_1), then, within this ensemble, simple first-order kinetics are given by the process

$$L \xrightarrow{k_U} S_1, \tag{4-3}$$

where L is the looped state, S_1 is the state of the DNA with only one operator bound to a protein, and k_U is the unlooping rate. Therefore, the time-dependent probability of unlooping is

$$S_1(t) = 1 - e^{-k_U t}, \tag{4-4}$$

which corresponds to the fit function (Eq. 4-1) for the lifetimes of the looped state. The kinetics of loop formation, however, is more complicated because there are different unlooped substates that cannot be distinguished within our experiment. We start by collecting all time intervals that begin at an unlooping event and end with the formation of a loop. The kinetics may be represented as

$$S_2 \underset{k_-}{\overset{k_+}{\rightleftharpoons}} S_1 \xrightarrow{k_L} L, \tag{4-5}$$

where S_1 is the state of one vacant and one occupied operator and may directly convert to the looped state L at a rate k_L, or remain unlooped and convert to state S_2 at a rate k_-. State S_2, however, is an alternate configuration with both or neither operator occupied by a protein, which is not able to directly form a loop, but may convert to state S_1 at a rate k_+. With the initial condition, the first-order kinetics above may be solved for the time-dependent probability of forming a loop

$$L(t) = 1 - \frac{1}{2\alpha}\left[(\kappa - k_L + \alpha)e^{-t/\tau_1} - (\kappa - k_L - \alpha)e^{-t/\tau_2}\right], \tag{4-6}$$

where $\kappa = k_+ + k_-$, $\alpha = \left[(\kappa + k_L)^2 - 4k_+k_L\right]^{1/2}$, and the time constants are defined as $\tau_1 = 2/(\kappa + k_L - \alpha)$ and $\tau_2 = 2/(\kappa + k_L + \alpha)$. Equation 4-6 is again a biexponential distribution and corresponds to the fit function of Eq. 4-2. Therefore, we can unambiguously extract the four rate constants in our kinetic model. The results are shown in Table 4-2

and plotted in Figure 4-3. Our main observation is that, within the uncertainties of our measurements, k_+, k_-, and k_U are independent of force whereas k_L is acutely force sensitive on the hundred-femtonewton scale. This is consistent with the conventional expectation that the rate of conversion between the unlooped states S_1 and S_2 does not vary significantly as a function of the stretching force on this scale. The insensitivity to applied force of the unlooping rate k_U can be explained by considering the binding energy of the LacI protein to the DNA, whose disassociation from the lac binding site is necessary to break a loop. With a binding energy of 10^{-19} J[82] and an operator region that spans ~20 bp, the minimum force needed to remove the protein from the operator is ~10 pN, which is several orders of magnitude greater than the tension we applied. It is clear then why the looped state is relatively insensitive to mechanical tension. On the other hand, the sensitivity of the looping rate to such small forces is quite striking and potentially rich in implications. Since the characteristic force that results from thermal fluctuations of ds-DNA is approximately 80 fN, and since DNA looping is a result of thermal fluctuations, femtonewton forces can clearly impact the loop formation process.

Table 4-2 Fits to the cumulative probability distributions.

Force (fN)		60 ± 5	78 ± 6	121 ± 9	183 ± 15
Kinetic Rate (10^{-3}/s)	k_U	48.1 ± 0.6	44.5 ± 0.4	41.5 ± 0.6	40 ± 1
	k_L	262 ± 7	196 ± 6	79 ± 1	32 ± 1
	k_-	61 ± 9	48 ± 5	21 ± 2	25 ± 4
	k_+	40 ± 10	24 ± 5	14 ± 2	21 ± 3

4.3.2 DNA loop topology

Quantitatively useful models of loop formation must explicitly consider the orientation of the operators along the DNA in the looped state, as the exact geometry of the loop matters significantly. Such theories were developed by Blumberg *et al.*[35,36] and, independently, by Yan *et al.*[79]. In this study we use the model developed by Blumberg *et al.* so begin by finding the difference in the force dependent contributions to the free energy between a looped and a stretched length of DNA: $\Delta F = F_L(f,\theta) - F_S(f)$. The kink angle θ is defined as the angle between the tangent vectors of the DNA at the operator sites of the protein-DNA complex. A relation for the excess contribution to the free energy as a function of kink angle, imposed on the DNA by the loop, is given by:

$$F_L = \frac{4 f^{1/2}[1-\cos(\theta/4)]}{1+12 f^{-3/2}[1-\cos(\theta/4)]/[1+\cos(\pi-\theta)]}, \tag{4-7}$$

where the free energy is in units of k_BT and the force f is in a loop units of the characteristic force for thermal fluctuations, $f_c = k_BT/l_p \approx 80$ fN.

An analytic relation for the free energy of a stretched segment of DNA is given by the difference between the potential energy of a wormlike chain and the work done by tension:

$$F_S = -\frac{l_l x^2}{4}\left(\frac{1}{(1-x)^2}+2\right), \tag{4-8}$$

where l_l is the loop length of the DNA and x is the relative extension of the DNA in units of l_p. We can now calculate the characteristic time necessary to form a loop under an applied force using the principle of detailed balance

$$\frac{\tau_f}{\tau_0} = e^{-\Delta F}, \tag{4-9}$$

where τ_0 is the characteristic time at zero force.

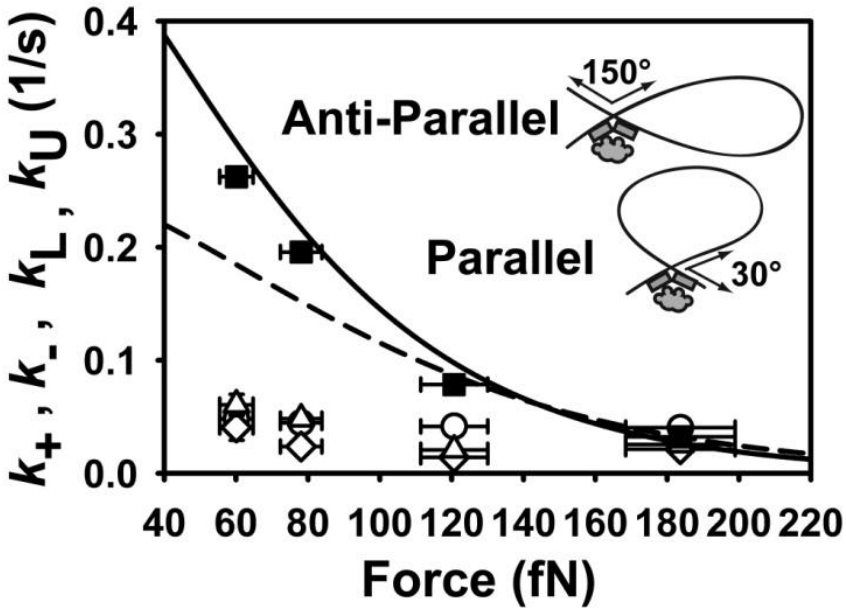

Figure 4-3 Measured values for k_- (Δ), k_+ (◊), k_L (■), and k_U (○) (see Table 4-2). The looping rate k_L is fit by the theoretical predictions for the antiparallel (solid line) and parallel (dashed line) topologies illustrated in the insert.

X-ray studies of the co-crystals of LacI protein bound to short operator fragments have revealed the structure of the DNA protein complex[24]. These results impose constraints upon, but do not fully determine the topology of the DNA loop. The preferred direction in which the DNA enters and leaves the looped complex remains unsettled, but the corresponding topologies are either antiparallel conformations, with a kink angle of approximately 150°, or parallel conformations, with a kink angle of 30°. To fit the data, we calculate $\tau_f = 1/k_L$ from Eq. 4-9 as a function of force using the wormlike chain model to provide the relative extension x in Eq. 4-8. Since we cannot directly measure the force

free lifetime τ_0, we use this as a single adjustable parameter to fit the curves. The value for τ_0 is given by a least squares fit to the data. We then generate a curve for both the antiparallel and parallel conformations and see, from Figure 4-3, that the antiparallel topology is more force-sensitive than its parallel counterpart is. Our data suggest that the antiparallel conformation is the dominant topology of a generic LacI-mediated DNA loop.

In conclusion, our results establish that very small forces, on the order of a hundred femtonewtons, can control the assembly of the regulatory protein-DNA complex necessary for expression of the lac gene. On the other hand, once formed, the looped complexes are quite stable and cannot easily be disrupted by tension in the substrate DNA, giving the system much-needed robustness. Thus, it appears more than likely that mechanical pathways can control transcription through the application of tiny forces that are generated by other intracellular processes. We hope that the development of force measurement techniques inside living cells will lead to the identification of such pathways. We also conclude that such regulatory forces would likely act on the assembly process of these complexes, but not their breakdown.

Chapter 5

Protein-Mediated DNA Loop Formation and Breakdown in a Fluctuating Environment

Living cells provide a fluctuating, out-of-equilibrium environment in which genes must coordinate cellular function. DNA looping, which is a common means of regulating transcription, is very much a stochastic process; the loops arise from the thermal motion of the DNA and other fluctuations of the cellular environment. We present single-molecule measurements of DNA loop formation and breakdown when an artificial fluctuating force, applied to mimic a fluctuating cellular environment, is imposed on the DNA. We show that loop formation is greatly enhanced in the presence of noise, yet find that hypothetical regulatory schemes that employ mechanical tension in the DNA–as a sensitive switch to control transcription–can be surprisingly robust due to a fortuitous cancellation of noise effects.

5.1 Introduction

Genes operate within a crowded cellular environment that is constantly interacting with the encoding DNA through various proteins and enzymes that bind along its contour, through tension induced by chromosomal packing, etc.[83-85]. We are only beginning to un-

derstand how a crowded and fluctuating cellular interior affects genetic regulation; however, the cytoskeleton of eukaryotes already provides a startling example of the dynamic effects of the intracellular medium[86-88]. The cytoskeleton, whose mechanical properties are critical to many cellular processes, is often considered an active polymeric gel, since its organization is driven by ATP hydrolysis, and is known to generate mechanical stress and shear forces. Its active properties give rise to non-equilibrium effects such as the generation of an "effective temperature" that can drive processes of embedded elements beyond the levels of thermal activation. Recently, force fluctuations an order of magnitude larger than thermal fluctuations have been measured within the cytoskeleton[89]. Such findings remind us that, the cellular interior is very much an active, non-equilibrium medium, the effects of which need to be given careful consideration.

A regulatory mechanism that is potentially acutely sensitive to environmental noise is the fluctuation driven formation of protein-mediated loops. In genomic DNA, this is a ubiquitous motif for the transcriptional control of gene expression[12]. The lac operon, which is responsible for efficiently metabolizing lactose in *E. coli* bacteria, provides a canonical example of DNA looping. A lac repressor-mediated DNA loop is formed when tetrameric *lac* repressor (LacI) protein simultaneously binds to two lac operator sites and is crucial for the repressive regulation of lac genes[16]. Thermal fluctuations, which generate tiny entropic forces on the order of only $k_B T / l_p \approx 80\ \text{fN}$, where $l_p = 50\ \text{nm}$ is the persistence length[34,36], are sufficient to form loops within the DNA, making the association rate of loops extremely sensitive to tension along the DNA molecule[31]. Nonetheless, these loops must regulate transcription within a crowded cellular environment that is constantly interacting with the DNA through various proteins and enzymes that bind along

its contour, through tension induced by chromosomal packing, etc.[83-85]. Moreover, the interior of the cell is known to have regions of varying temperature due to active processes such as enzyme catalysis and metabolic activity[90].

5.2 Materials and Methods

To explore the effects of environmental fluctuations on protein-mediated DNA loops, a 1316 bp dsDNA molecule with two primary lac operators spaced 305 bp apart was tethered to a cover glass and then attached to an 800 nm polystyrene microsphere. The microsphere was then trapped within the linear region of the optical potential of a focused laser beam allowing us to apply a well-defined tension to the DNA, as shown in Figure 5-1. Details of our axial-constant force optical tweezers as well as a discussion of the DNA preparation can be found in Ref.[75]. Tension in the DNA was calibrated to include both the applied optical force, which is linearly proportional to the laser intensity modulated by an acousto-optic modulator (AOM), and volume exclusion effects arising from entropic interactions between the microsphere and the cover glass[63]. The looped and unlooped states of the DNA molecule, which correspond to different axial positions of the microsphere, were measured by analyzing defocused images acquired on a CCD camera at 100 fps in the presence of 100 pM of LacI protein. This method provides excellent temporal resolution for detecting loop formation and breakdown events with time windows as short as 300 ms.

Fluctuating forces were applied to the DNA by modulating the intensity of the trapping laser with an AOM connected to a data acquisition board and controlled by a custom LabVIEW program. The program generated Gaussian white noise, at a sampling rate of $1/\delta t$, which was superimposed upon a set average optical force, h (see Figure 5-1). The

modulation was performed such that the force applied to the trapped microsphere was randomly chosen from a normalized Gaussian distribution of standard deviation σ.

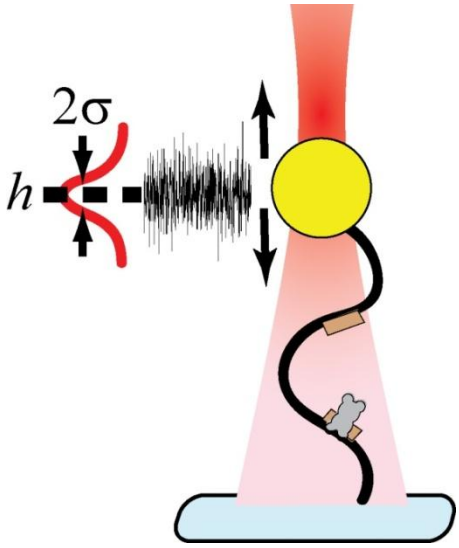

Figure 5-1 Tethered microsphere trapped in the linear region of the optical potential and stretched by fluctuating forces. Gaussian white noise with standard deviation σ is superimposed upon a set average optical force, *h*.

Since it is the tension along the DNA that we would like to display white noise statistics, we must first determine how flat a spectrum can be generated by optically shaking the microsphere. The time-evolution of the tension induced in the DNA from fluctuating the laser intensity may be approximated from the following differential equation:

$$\gamma \frac{d\varepsilon}{dt} = -\kappa\varepsilon + \xi(t), \tag{5-1}$$

where ε is the location of the center of the microsphere, κ is the spring constant of the DNA, $\gamma = 6\pi\eta r$ is the hydrodynamic friction coefficient of the microsphere, η is the viscosity of the medium and *r* is the radius of the microsphere. $\xi(t)$ is the applied stochastic driving force and, so long as δt is sufficiently small, may be treated as delta-correlated

white noise, i.e.: $\langle \xi(t)\xi(t') \rangle = 2\alpha\delta(t-t')$, where $2\alpha = \sigma^2 \delta t$. The resulting time correlation of the induced tension is then effectively low-pass filtered:

$$\langle \eta(t)\eta(t') \rangle = \frac{2\alpha}{\tau_c} e^{-|t-t'|/\tau_c}, \tag{5-2}$$

where $\eta(t) = \kappa\varepsilon(t)$, with a characteristic time $\tau_c = \gamma/\kappa$. If we only consider events that happen on timescales greater than τ_c we may approximate the colored spectrum of Eq. 5-2 by purely white noise such that Eq. 5-2 reduces to $\lim_{\tau_c \to 0} \langle \eta(t)\eta(t') \rangle \approx 2\alpha\delta(t-t')$. From the worm-like chain model for DNA, τ_c ranges from 5-8 ms at tensions from 180-120 fN. Therefore, if we set δt below the cutoff imposed by τ_c (for our experiments, we fix δt at 2 ms ($1/\delta t$ = 500 Hz)) then the applied fluctuations are essentially white up to frequencies $1/\tau_c$, and we may adjust the strength of the noise by tuning the width of the distribution σ. It is more intuitive, perhaps, to consider the applied fluctuations as generating an additional energy contribution to the thermal modes of the DNA of magnitude $k_B T_\alpha = \sigma^2 \delta t / 2\gamma$, to parametrize the fluctuations relative to the ambient temperature of thermal fluctuations T_α / T.

5.3 Experimental Results

Figure 5-2 shows the distribution of lifetimes for the looped and unlooped states at a mean tension of 153 fN and with fluctuations of T_α/T = 0, 0.01, 0.05, and 0.12. As indicated in the figure, the lifetimes of the looped state are independent of the fluctuations. This is consistent with previous findings that the looped state is insensitive to femtonewton forces[31]. The lifetime of the unlooped state, however, is clearly seen to decrease as we increase the fluctuations. At 2σ, approximately 95% of the noise distribution is accounted

for. Since volume exclusion forces are on the order of 35 fN[63], σ = 60 fN or T_α/T = 0.12 are the largest fluctuations we can apply to the DNA without significantly clipping the distribution.

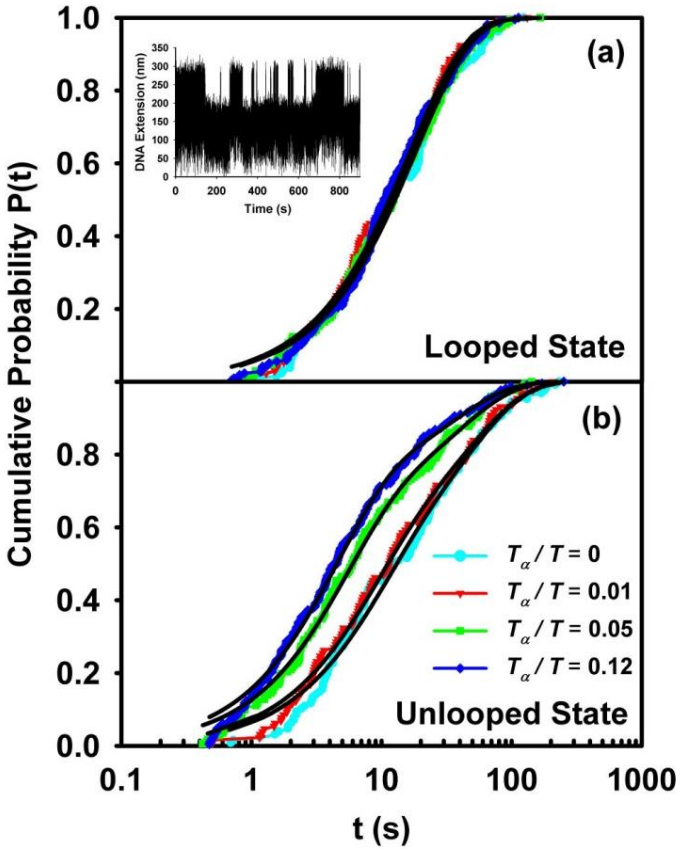

Figure 5-2 Experimental measurements of the (a) looped and (b) unlooped cumulative probability distributions for various noise conditions (right to left: T_α/T = 0, 0.01, 0.05, 0.12) at a mean tension of 153 fN. The data clearly show that the looped lifetimes are unaffected by the applied noise and that the unlooped lifetimes decrease with increasing noise levels. The solid lines are exponential (biexponential) fits to the looped (unlooped) data. The insert to (a) shows a typical raw trace of the DNA extension vs. time.

We fit the cumulative probability distributions using the kinetic scheme detailed in Ref.[31] to extract loop dissociation and association lifetimes. In summary, the looped lifetimes are simply fit by a single exponential function parameterized by the looped lifetime

τ_L: $1-\exp(-t/\tau_L)$. The unlooped kinetics, however, are more complicated, and may accurately be described by collecting all time intervals beginning with an unlooping event and ending upon the formation of a loop:

$$S_2 \underset{k_1}{\overset{k_2}{\rightleftharpoons}} S_1 \xrightarrow{k_L} L. \tag{5-3}$$

States S_1 and S_2 arise because there are multiple unlooped sub-states available to the protein-DNA system. S_1 represents a state with only one occupied operator, which may either loop at rate k_L to form state L, or remain unlooped and convert at rate k_1 to state S_2. State S_2 is an alternate configuration with both or neither operator occupied, which cannot form a loop, but may convert back to state S_1 at a rate k_2. The first-order kinetics results in the following biexponential function for the cumulative probability distribution:

$$L(t) = 1 - \frac{1}{2\alpha}[c_+ e^{-t/\tau_-} - c_- e^{-t/\tau_+}], \tag{5-4}$$

where $\kappa = k_2 + k_1$, $\alpha = \left[(\kappa + k_L)^2 - 4k_2k_L\right]^{1/2}$, $c_\pm = (\kappa - k_L \pm \alpha)$ and the time constants are defined as $\tau_\pm = 2/(\kappa + k_L \pm \alpha)$. From this fit equation we are able to extract the unlooped lifetime $\tau_u = 1/k_L$. In accord with the constant force results[31], the interconversion rates k_2 and k_1 were found to be essentially independent of the applied tension.

Figure 5-3 displays the unlooped lifetimes as a function of the noise T_α/T normalized to the zero noise lifetime, $\tau_u(h;T_\alpha/T)/\tau_u(h;0)$, about a mean applied tension of 153 fN. The results demonstrate that fluctuations do indeed drive loop formation as the rates are substantially enhanced as the noise increases to levels comparable to typical thermal fluctuations in DNA. These results coalesce nicely with previous observations that femtonewton forces can radically affect the rate at which LacI-mediated DNA loops form

Ref.[31]. Our results imply that it requires an excess energy of only 5% of $k_B T$ to double the rate at which DNA loops form, which is only a fraction of that which the cytoskeleton can induce upon an embedded polymer. This stochastic mechanism might provide an alternate 'noisy' means for mechanical control of genetic transcription.

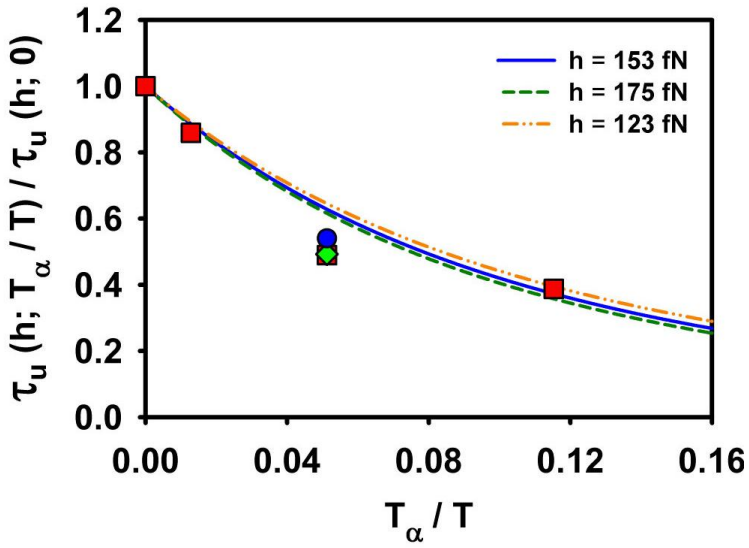

Figure 5-3 Normalized unlooped lifetimes as a function of applied noise. The (square) data points were taken at a mean tension of h = 153 fN. The (diamond) and (circle) data points were taken at h = 123 and 175 fN respectively. The three data points measured at a constant applied noise (T_α/T = 0.05) but different mean tension (h = 123, 153, 175 fN) show that the normalized lifetimes are insensitive to the average tension. The lines are the theoretical curves, shown for h = 123, 153, 175 fN, given by Eq. 5-9 with the replacement of an effective temperature $T \to T_E$.

Although the rate at which DNA loops form is quite sensitive to environmental fluctuations, our data also show that this sensitivity is practically independent of the mean applied tension in the DNA. A separate measurement of the loop formation rate as a function of mean tension, h = 123, 153, and 175 fN, collected at a constant applied noise, T_α/T = 0.05, reveals a striking observation: the normalized lifetimes, $\tau_u(h;0.05)/\tau_u(h;0)$, are constant with an approximate value of 0.5 irrespective of the average tension h in the

molecule (see Figure 5-3). As we will show, this could allow regulatory schemes that are based upon protein-mediated DNA loops to display a significant level of robustness to noise.

5.4 Modeling Results

One might imagine that the increase in looping occurs because the fluctuations allow the random sampling of a low tension regime. However, any increase in looping gained by reducing the tension is negated by the equally likely sampling of high tension fluctuations, requiring us to consider the role of fluctuations in more detail. To understand the effects of noise on the rate of loop formation, we have developed a phenomenological model of the looping process. We begin with an effective Langevin equation for the motion of the tethered particle system:

$$\gamma \frac{dx}{dt} = -\frac{dU(x;h)}{dx} + \xi(t). \tag{5-5}$$

The variable $x(t)$ describes diffusion along the energy landscape provided by $U(x; h)$. The stochastic term $\xi(t)$ accounts for thermal fluctuations and is modeled as a white noise source with zero mean, i.e., $\langle \xi(t)\xi(t') \rangle = 2\lambda\delta(t-t')$, with $\lambda = \gamma k_B T$.

We choose the following phenomenological form for the energy barrier:

$$U(x;h) = \frac{1}{2}ax^2 - \frac{1}{3}bx^3 + hx. \tag{5-6}$$

The harmonic term contains the cost of bending the DNA, while the cubic term, although somewhat arbitrary, is the simplest contribution that can give rise to an energy barrier between a second equilibrium state, which is here assumed to be the looped configuration, see Figure 5-4. The linear term represents the force h that we apply with optical

tweezers to stretch the DNA, which effectively modulates the energy barrier by tilting the energy landscape and, therefore, increasing or decreasing the barrier height ΔU. Note that we are not attempting to account for the unlooping process, since the looped state, as our data reveal, is not sensitive to the forces we apply.

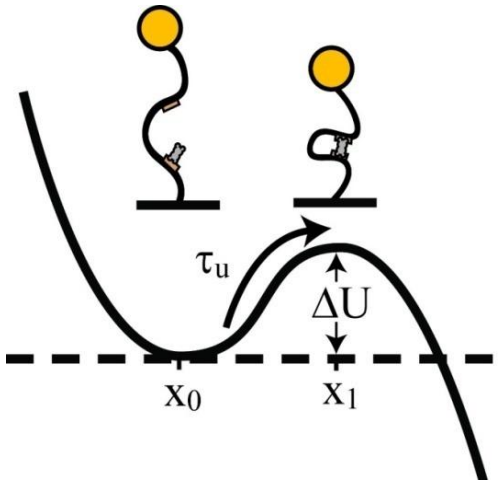

Figure 5-4 The loop association process can be modeled by diffusion over a barrier. The unlooped lifetime τ_u is given by the average time it takes for the DNA to diffuse from the equilibrium position x_0, within the energy landscape, to the top of the energy barrier, of magnitude ΔU at x_1 , where it forms a looped state.

An exact formula for the mean passage time[91] across the energy barrier from x_0 to x_1 is given by

$$\tau_u = \frac{\gamma}{k_B T}\int_{x_0}^{x_1} dx \exp\left(\frac{U(x;h)}{k_B T}\right)\int_{-\infty}^{x} dy \exp\left(\frac{U(y;h)}{k_B T}\right). \tag{5-7}$$

If the potential barrier ΔU is large compared to $k_B T$, then Eq. 5-7 can be expanded about the vicinity of x_0 and x_1 to yield the Kramers formula for the unlooped lifetime

$$\tau_u = \frac{2\pi\gamma}{\sqrt{U''(x_0;h)\left|U''(x_1;h)\right|}}\exp\left[\frac{\Delta U}{k_B T}\right], \tag{5-8}$$

where $\Delta U = U(x_1;h) - U(x_0;h)$. From Eq. 5-6, we can rewrite this relation as

$$\tau_u = \frac{2\pi\gamma}{\sqrt{a^2 + 4bh}} \exp\left[\frac{\left(a^2 + 4bh\right)^{3/2}}{6b^2 k_B T}\right], \tag{5-9}$$

We must now determine the coefficients *a* and *b* that parameterize our model potential (Eq. 5-6). We do this by an iterative least-squares fit of the lifetimes, given by Eq. 5-7, to our constant force (zero fluctuation) data, the result of which is shown in Figure 5-5. We have found the difference in the resulting fit parameters to be negligible between the exact, Eq. 5-7, and approximate Kramers relation, Eq. 5-9. It should be noted that the parameter *a* is quite different from the spring constant κ of a worm-like chain model since *a* must parameterize the full three-dimensional search of the polymer to form a loop within this lower dimensional, effective energy landscape.

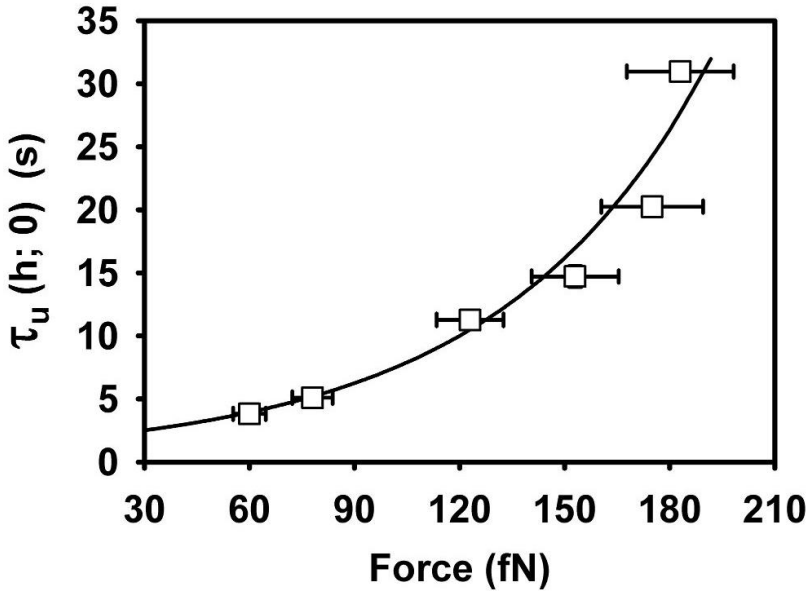

Figure 5-5 Unlooped lifetime τ_u as a function of a constant applied force. The solid line is the theoretical fit, given by the Kramers relation of Eq. 5-9 to the data points (squares). The coefficients of the potential *U(x; h)* are $a = 4.64 \times 10^{-5}$ N/m and $b = 739$ N/m^2.

Since we add noise to the system by linearly modulating the tension applied to the DNA, we may incorporate this additional noise by modifying the correlations of the stochastic source $\xi(t)$ such that $\lambda = \gamma k_B T_E$, where we have introduced the effective temperature

$$T_E = T\left(1 + T_\alpha / T\right). \tag{5-10}$$

With the replacement $T \to T_E$ in Eq. 5-9 we are able to account for the effects of noise on the unlooped lifetimes $\tau_u\left(h; T_\alpha / T\right)$ at a mean tension *h*. This model gives excellent agreement with our experimental measurements of the looping lifetime $\tau_u\left(h; T_\alpha / T\right)$ as a function of noise (see Figure 5-3). Furthermore, it predicts robustness to noise similar to what we observe experimentally (see Figure 5-3). The theory predicts a fairly constant ratio $\tau_u\left(h; 0.05\right) / \tau_u\left(h; 0\right)$ = 0.65, 0.63, and 0.62 at a mean tension *h* = 123, 153, and 175 fN, respectively.

5.5 Discussion

Our results suggest how a force dependent genetic switch that employs DNA looping to regulate transcription could operate stably within a noisy environment. For instance, consider a regulatory element controlled by the formation of a DNA loop at a basal rate k_{t1} under constant tension h_1 (Figure 5-6). A regulatory signal could be provided by a change in tension, h_2, such that the loop formation rate is now a factor of *p* times the basal rate, i.e. $k_{t2} / k_{t1} = p$. If we assume that the tension felt by the DNA fluctuates around the targets t_1 and t_2 such that we have two new looping rates $\tilde{k}_{t1}$ and $\tilde{k}_{t2}$, our results imply

that $\tilde{k}_{t1}/k_{t1} = \tilde{k}_{t2}/k_{t2}$, which means that $\tilde{k}_{t2}/\tilde{k}_{t1} = p$, so that the expression signal is unaffected by the noise.

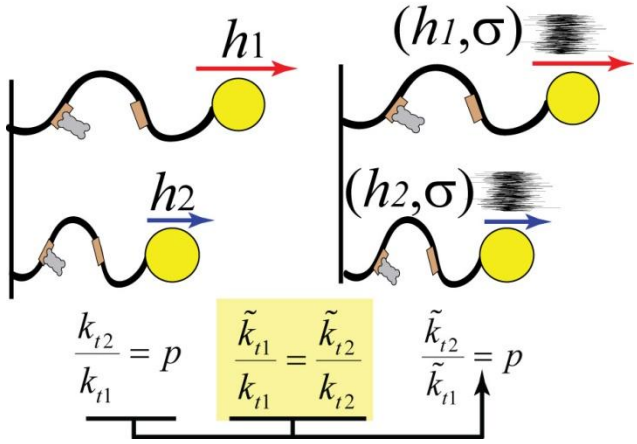

Figure 5-6 Schematic showing how hypothetical regulatory schemes that employ mechanical tension in DNA to control transcription can be surprisingly robust even in the presence of fluctuations. As explained in the text, since our results imply that $\tilde{k}_{t1}/k_{t1} = \tilde{k}_{t2}/k_{t2}$, a force dependent genetic switch is unaffected by the noise.

We have demonstrated how noise from thermal and environmental fluctuations drives protein-mediated DNA loop formation, yet leaves the loops unaffected once formed. Environmental fluctuations only a fraction of the size of thermal fluctuations in the DNA can greatly enhance the rate at which these loops form. We interpret the results with a fluctuating barrier model that can quantitatively explain and predict our measurements. This model is based on the previously demonstrated sensitivity of loop formation to static mechanical tension, which led to the suggestion that cells may utilize tension to regulate transcription through mechanical pathways, as opposed to the more commonly considered biochemical ones[31]. Based on our new observations, we may now postulate the feasibility of an alternate mechanical regulatory mechanism that uses environmental fluctuations as a means to control transcription. Furthermore, we have shown that the sensitivity

of loop formation to fluctuations is insensitive to baseline static mechanical tension, and have demonstrated how this feature can lead to robustness in regulatory function.

Chapter 6

Bead Size Effects on Protein-Mediated DNA Looping in Tethered-Particle Motion Experiments

Tethered particle motion (TPM) has become an important tool for single-molecule studies of biomolecules. We investigate the effect of the attached microsphere on the formation and breakdown of protein-mediated DNA loops in the lac repressor system by comparing data from a conventional TPM experiment with 800 nm polystyrene beads and darkfield TPM using 50 nm Au nanoparticles. We found that the lifetimes of the looped and unlooped states are extended less than two-fold by the presence of the large bead, which is consistent with our expectation of weak excluded-volume effects and hydrodynamic surface interactions from the cover glass and microsphere.

6.1 Introduction

Tethered particle motion (TPM) is a simple and increasingly popular experimental technique to study protein-DNA interactions at the single molecule level. In TPM, the biomolecule of interest is attached at one end to a micro- scope cover glass and at the other end a marker, typically a polystyrene microsphere, is affixed[92]. The motion of the marker bead is observed by standard light microscopy to infer dynamical information

about the biomolecular sys- tem. To achieve good image quality, the marker bead of- ten has a radius of several hundred nanometers, which is comparable to or even larger than the contour length of the molecule under study. Therefore, a common concern is that the presence of such a large bead might affect the dynamics of the system of interest in a typical TPM experiment.

In this study, we explicitly study the effects of the marker bead on the rate constants of a biological process, namely DNA loop formation and dissociation. Our experimental results, which are in good agreement with the theoretical predictions of Segall et al.[63], show that bead size effects only contribute about a factor of 2 to the rate of loop formation, further validating TPM as a valuable method for studying protein-mediated DNA looping.

To assess the severity of such bead-induced effects, we have measured the formation and breakdown rates of lac repressor (LacI) mediated DNA loops in a modified TPM experiment that uses Au nanoparticles of only 50 nm in diameter, and compared the results to data from more conventional TPM experiments that use 800 nm polystyrene microspheres. This system was chosen not only because it is fairly representative of a typical TPM experiment, but also because the loop formation process is thought to be acutely sensitive to tension in the DNA[14,79], which might arise from attachment to a large microsphere. Admittedly, many TPM experiments are able to employ a microsphere of half the size we have chosen; however, if the probe effects the looping process we would like these effects to be clearly indicated by our data so have chosen a fairly large microsphere.

6.2 Materials and Methods

For the TPM experiments, we synthesized a 790 bp end- labeled ds-DNA fragment containing two LacI-binding operator sites 320 bp apart by polymerase chain reaction (PCR). The DNA is tagged with either Au nanoparticles or polystyrene microspheres and is then tethered to a micro- scope cover glass within a sample chamber containing a 200 pM solution of LacI protein.

6.2.1 Tethering protocol

The PCR primers are modified with biotin and digoxigenin, respectively. The end-labeled DNA is incubated with either streptavidin coated Au nanoparticles (Nanocs Inc.) radius R_B = 25 nm, or streptavidin coated polystyrene microspheres (Spherotech) R_B = 400 nm, with relative concentrations of approximately 1:10, in a 50 µl volume of PTC1 buffer (20 mM Tris-Acetate, pH 8.0, 130 mM KCl, 4 mM $MgCl_2$, 0.1 mM EDTA,0.1 mM DTT, 20 µg/ml BSA, 80 µg/ml Heparin, 1 mg/ml α-casein). The excess of beads prevents the formation of multiple DNA tethers. The DNA-bead mixture is incubated for 30 min at 5°C on a rotating rack. Sample chambers consisting of a microscope slide, a cover glass, and a parafilm spacer are washed with 200 µl phosphate buffered saline (PBS) buffer (137 mM NaCl, 10 mM Phosphate, 2.7 mM KCl, pH 7.4) and then filled with 20 µg/ml anti-digoxigenin (polyclonal from sheep, Roche Scientific) to coat the slide with anti-bodies. Excess antibodies in the solution are washed away with 200 µl PTC1. Continued incubation with PTC1 for half an hour blocks the surface against non-specific binding. The DNA-bead mixture is then pipetted into the sample chamber and incubated for 5min. The excess beads are washed away with 400 µl PTC1. The buffer is replaced with LBB buffer (10 mM Tris-HCl, pH 7.4, KCl 200 mM, EDTA 0.1 mM, α-

casein 1 mg/ml, DMSO 0.05 v/v, DTT 0.2 mM) by pipetting 200 µl into the chamber. Finally, 100 µl of a 200 pM solution of LacI protein in LBB is introduced into the chamber.

6.2.2 Imaging and analysis

The tethered nanoparticles are imaged by darkfield microscopy on a Zeiss Axiovert S100 inverted microscope that is custom fitted with an Olympus U-DCW darkfield condenser (oil, N.A. 1.2-1.4) and a 100x Olympus UPlan- FLN (oil, N.A. 0.6-1.3) darkfield objective. The polystyrene microspheres are imaged by brightfield microscopy using the same objective. All images are acquired at 30 ms intervals on a Cascade 650 cooled CCD camera (Photometrics). At this frame rate the influence of time averaging by the detector should be negligible. The particles are tracked with custom MATLAB software that implements a Gaussian mesh algorithm to locate the center of each nanoparticle[93]. With this algorithm we are able to determine the beads center with an error of less than 5nm[14]. The resulting radial coordinates are then filtered with a 0.05 Hz Butterworth filter to remove slow drift.

Figure 6-1 provides an example of the data obtained from measurements with Au nanoparticles and polystyrene microspheres. Loop formation and breakdown events are readily visible in the time traces. The looped and unlooped states are also quite evident in the double-peaked histograms of the motion of the markers. The lifetimes of the looped and unlooped states can be extracted from these traces by performing a running average over the xy motion of the bead and then using a simple thresholding algorithm to detect looping and unlooping of the DNA. By fitting Gaussians to the looped and unlooped distributions displayed in the histogram, the threshold was chosen at the minimum between

the peaks of the two distributions. The resulting rates were fairly insensitive to the exact location of the threshold; a 10% shift in the threshold from the fitted location resulted in only a < 5% change in the kinetic rates. Data was acquired for 20 minutes for each of 7 tethered Au nanoparticles and 7 tethered polystyrene microspheres. Slight quantitative differences in the looping and unlooping rates, of roughly 10-15%, where found when we varied the window size from 1-3 s.

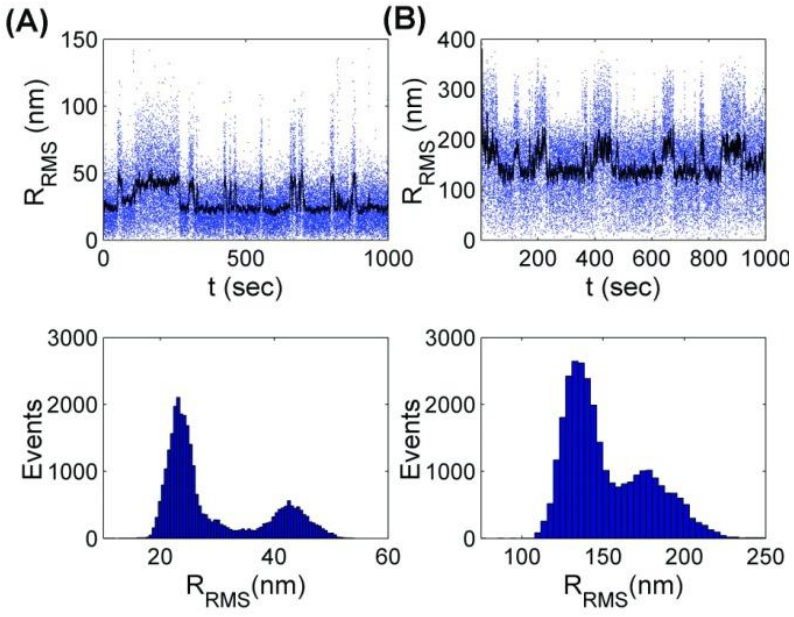

Figure 6-1 Looping data for (A) Au nanoparticles and (B) polystyrene microspheres. The uppermost plots show the root mean square displacements as a function of time. The black lines result from averaging over a moving window of 2 s. The lower plots are histograms of the averaged motion showing two distinct states.

6.3 Experimental Results

The extracted dwell times for the looped and unlooped states are pooled as cumulative probability distributions as shown in Figure 6-2.

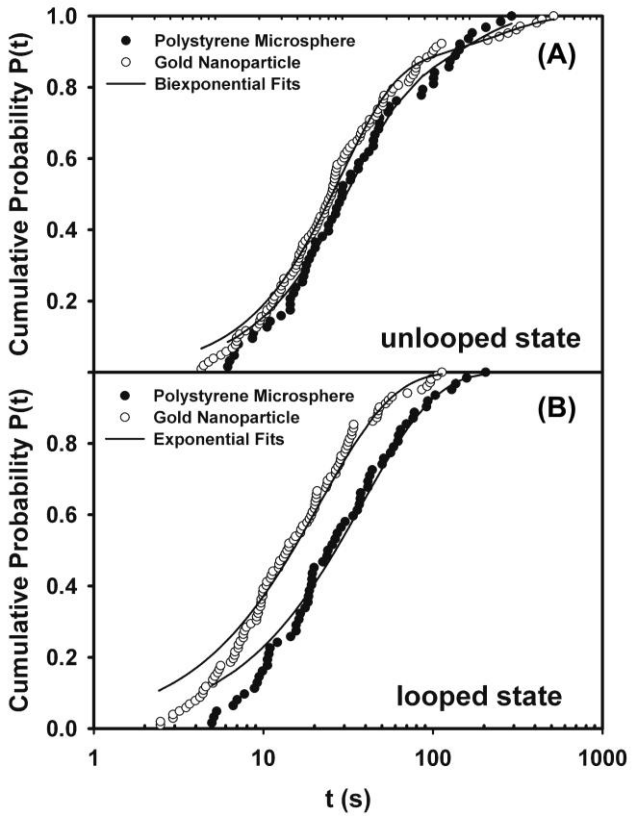

Figure 6-2 The data of (A) the unlooped state and (B) the looped state are fit to the biexponential function of Eq. 6-2, and the single exponential function of Eq. 6-1, respectively. For the un- looped state τ_1 = 150 ± 70 s, τ_2 = 8.6 ± 0.4 s, and c = 0.15 ± 0.03 for the Au nanoparticles and τ_1 = 80 ± 40 s, τ_2 = 10 ± 1 s, and c = 0.25 ± 0.09 s for the polystyrene microspheres. For the looped state τ = 21.5 ± 0.7 s for the Au nanoparticles and τ = 38 ± 2 s for the polystyrene microspheres.

The loop breakdown data was well fit by a single exponential function of the form

$$P(t:\tau) = 1 - e^{-t/\tau}, \tag{6-1}$$

with lifetime τ. The loop formation data, however, could not be fit by a single exponential, but was well fit by a double exponential function. This has been observed previously[13] and is the result of there being a multiplicity of available protein occupancy configurations comprising the unlooped state. We, therefore, fit the loop data with the following biexponential function:

$$P_2(t:\tau_1,\tau_2) = cP(t:\tau_1) + (1-c)P(t:\tau_2), \quad (6\text{-}2)$$

with lifetimes τ_1 and τ_2 and a dimensionless weight constant c. The fits are displayed in Figure 6-2. Loop formation and breakdown are both faster when the Au nanoparticle is used instead of the microsphere. The effect is small for the loop formation process, and amounts to a factor of about two in the loop breakdown rate.

The relatively good agreement between the different experiments is particularly noteworthy because they were conducted in very different regimes: the dynamics of the DNA-particle construct is dominated by the intrinsic dynamics of the DNA in the nanoparticle case, whereas the motion of the microsphere dominates in the other experiment. To distinguish these two regimes, Segall *et al.*[63] introduced a dimensionless parameter, the "excursion number", which is essentially the ratio of the friction coefficients of the bead to that of the DNA, $N_R \equiv R_B \Big/ \left(l_c l_p/3\right)^{1/2}$, where R_B is the radius of the bead, l_c is the contour length of the DNA, and l_p is the persistence length of the DNA. For the Au nanoparticles, the excursion number is N_R = 0.3 so the dynamics is mostly DNA-dominated, whereas N_R = 6.0 for the polystyrene microspheres indicates bead- dominated motion.

6.4 Discussion

6.4.1 Kinetic model

To further interpret our observations, we begin by developing a kinetic model for the underlying processes of loop formation and dissociation. Let us first consider the case of the looped state. If we collect all time intervals that start with a loop formation event and end at a loop breakdown event, then, within this ensemble, the kinetics are given by

$$L \xrightarrow{k_U} S_1, \tag{6-3}$$

where L is the population in the looped state, S_1 is the population in the unlooped state, and k_U is the unlooping rate. This can be translated into the following set of coupled differential equations:

$$\frac{dL}{dt} = -k_U L, \tag{6-4}$$

$$\frac{dS_1}{dt} = k_U L. \tag{6-5}$$

Under the initial condition $L(0) = 1$ these equations yield for the time-dependent probability of unlooping

$$S_1(t) = 1 - e^{-k_U t}. \tag{6-6}$$

By comparison with Eq. 6-1, of the looped state fit to the data

This result justifies the single exponential fit, Eq. 6-1, of the looped state. The kinetics of loop formation is more complicated because there are different unlooped sub-states that cannot be distinguished within our experiment. We start by collecting all time intervals that begin at an unlooping event and end with the formation of a loop. The kinetics of loop formation within this ensemble may be written as follows:

$$S_2 \underset{k_-}{\overset{k_+}{\rightleftharpoons}} S_1 \xrightarrow{k_L} L. \tag{6-7}$$

S_1 is the state of one vacant and one occupied operator and may directly convert to the looped state L at a rate k_L, or remain unlooped and convert to state S_2 at a rate k_-. State S_2, however, is an alternate configuration with both or neither operator occupied by a protein, which is not able to directly form a loop, but may convert to state S_1 at a rate k_+. Our in-

terest in this study is not to explore the phase space of protein concentration as other groups have already carefully performed this study for constructs similar to the ones we employed here[78]. These results suggest that, at the 200 pM protein concentration we worked with, S_2 is most likely the state of both operators being unoccupied, however, this distinction does not affect the model. Once again, we may translate the kinetics into a set of coupled differential equations

$$\begin{aligned}\frac{dS_1}{dt} &= -\left(k_- + k_L\right)S_1 + k_+ S_2,\\ \frac{dS_2}{dt} &= -k_+ S_2 + k_- S_1,\\ \frac{dL}{dt} &= k_L S_1.\end{aligned} \tag{6-8}$$

With the initial condition S_1 (0) = 1, these equations may be solved for the time dependent probability of forming a loop

$$L(t) = 1 - \frac{1}{2\alpha}\left[(\kappa - k_L + \alpha)e^{-t/\tau_1} - (\kappa - k_L - \alpha)e^{-t/\tau_2}\right], \tag{6-9}$$

where $\kappa = k_+ + k_-$, $\alpha = \left[(\kappa + k_L)^2 - 4k_+k_L\right]^{1/2}$, and the time constants are defined as $\tau_1 = 2/(\kappa + k_L - \alpha)$ and $\tau_2 = 2/(\kappa + k_L + \alpha)$. Equation 6-9 is a biexponential distribution, again justifying our earlier fit, Eq. 6-2. With this result, we can unambiguously extract the four rate constants in our kinetic model.

The advantage of this approach is that the rate constants are now physically meaningful. If we think of the looping process as equivalent to diffusion over a potential barrier, we may associate changes to the kinetic rates as resulting from either diffusion effects, which modify the diffusion constant, or potential effects, which alter the thermodynamic energy landscape. The rates k_+, k_- are independent of the potential barrier; however, they

are dependent upon diffusion variables such as the total protein concentration and hydrodynamics.

Table 6-1 Rate constants from the kinetic model for gold nanoparticle and polystyrene microsphere marker beads.

	Au	Polystyrene
$k_+ \times 10^3$ (1/s)	48.1 ± 0.6	44.5 ± 0.4
$k_- \times 10^3$ (1/s)	262 ± 7	196 ± 6
$k_L \times 10^3$ (1/s)	61 ± 9	48 ± 5
$k_U \times 10^3$ (1/s)	40 ± 10	24 ± 5

The looping, k_L, and unlooping, k_U, rates, which can now be extracted from the data and are of primary interest to us here, may depend on both potential and diffusion effects. The potential effects are apparent if we look at the distribution histograms, such as the one in Figure 6-1. In equilibrium, $K = n_L/n_U = k_L/k_U$, where n_U and n_L are the unlooped and looped population, respectively. However, $K^{Au}/K^{PS} \approx 2/3$, which shows that the equilibrium constants between the two cases, Au nanoparticles, K^{Au} and polystyrene microspheres, K^{PS}, differ. Diffusion should not affect the equilibrium properties, so this is a clear sign that potential effects are important for understanding bead size effects on TPM. This, of course, does not prove that diffusive effects are irrelevant to the kinetics of the system, which is a possibility we will return to. We first focus on enumerating the various contributions that might modify the potential landscape of the system.

6.4.2 Entropic boundary effects

To understand the comparatively subtle differences observed between the two experiments, possible ways in which the probe may affect the dynamics of protein-mediated

DNA loop formation and breakdown need to be considered. For instance, excluded-volume effects arise from the impenetrability of the bead and the cover glass. These geometric constraints give rise to an effective repulsive force between the bead and the cover glass, which in turn can affect loop formation and breakdown rates. An analytic form for this volume exclusion force[63], treating the DNA as a Gaussian chain and constraining the motion of the bead, but not the DNA, is given by

$$F_{eff} = \frac{k_B T}{\sqrt{\pi l_c l_p / 3}} \left(\frac{1 - e^{-N_R^2}}{erf\left((N_R)\right)} \right), \tag{6-10}$$

and experimentally confirmed by Chen *et al.*[81]. The magnitude of these volume exclusion forces for the polystyrene microspheres and the Au nanoparticles are 35 fN and 9 fN, respectively. The characteristic force scale for thermal fluctuations of the DNA, which drive the loop formation process, however, is $k_B T / l_p \approx 80$ fN. Therefore, excluded-volume forces that are smaller than this may be expected to play a concomitantly small role in affecting the kinetics of loop formation. A detailed calculation using the formalism proposed by Blumberg *et al.*[14] supports this assertion by suggesting a two-fold decrease in the loop formation rate from the Au nanoparticle to the polystyrene microsphere experiment. This is roughly in line with the observed factor of 1.3. The effect of excluded-volume forces on loop breakdown, however, is expected to be even smaller and would favor faster breakdown in the presence of the bigger microsphere, so cannot account for the observed breakdown data.

Another constraint that is imposed on the DNA in TPM experiments is that the DNA is typically attached to the cover glass and bead through flexible carbon linkers, which act as freely rotating swivel joints. This flexible attachment changes the number of ther-

mal modes avail- able to the DNA when compared to free or infinitely long DNA[62]. One might argue that the boundary condition at the probe end of the DNA differs between the two experiments, with the nanoparticle allowing the tagged end of the DNA to freely fluctuate while the large microsphere confines the orientation of the DNA to roughly a half plane, similar to the boundary condition at the cover glass. The extra constraint imposed by the large microsphere leads to a decrease in entropy that would tend to stretch the DNA, altering the loop formation and breakdown rates in a similar manner to the excluded volume forces previously discussed. This effect, therefore, also cannot account for the change observed in the loop breakdown rate.

6.4.3 Hydrodynamic effects

The effects considered in the last section all fall under the category of potential effects since they each somehow restrict the conformational space of the DNA. In this section, however, we turn our attention to diffusion effects on the looping rate. The proximity of the bead to the cover glass may have an appreciable influence on the loop breakdown kinetics through long-range hydrodynamic interactions as non-slip boundary conditions for fluid flow near a surface increase the hydrodynamic friction. This could provide an explanation for the two-fold increase in the lifetime of the looped state for DNA attached to a polystyrene bead as opposed to a Au nanoparticle. To break a loop the binding energy of the LacI protein to the operator[51], approximately 10^{-19} J, must be overcome by thermal fluctuations. We may assume that dissociation occurs at a rate

$$k_B \propto \frac{D}{\pi k_B T} e^{E/k_B T}, \tag{6-11}$$

where D is the diffusion constant of the DNA. Since $D \propto 1/\eta$, where η is the effective viscosity of the medium, the looping lifetime depends linearly upon the viscosity. As hydrodynamic friction increases in the presence of boundary walls, the thermal fluctuations of the DNA slow down, making dissociation less likely. To quantitatively estimate how hydrodynamic effects might affect the looping life- time, we can approximate the RMS distance $z_{RMS} = \sqrt{\langle z^2 \rangle}$ between the attachment point of the DNA to the bead and the cover glass in the experiment. Segall *et al.*[63] provide an approximate formula for $\langle z^2 \rangle$ that includes the excluded volume repulsion

$$\langle z^2 \rangle = \left(6 - \frac{4}{\sqrt{\pi}} \frac{N_R e^{-N_R^2}}{erf\left(N_R\right)} \right) \left(\frac{l_c l_p}{3} \right). \tag{6-12}$$

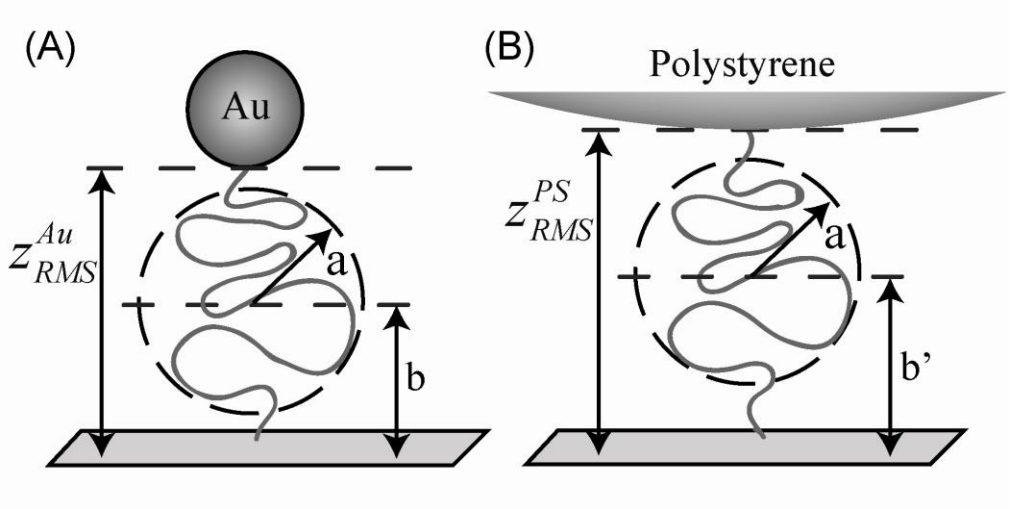

Figure 6-3 Hydrodynamic surface effects on the DNA. (A) DNA tethered by a gold nanoparticle is modeled by a sphere of effective radius at a distance $b = z_{RMS}^{Au}/2$ from a planar surface. (B) DNA tethered to a large polystyrene microsphere is modeled by DNA of the same effective radius *a*, at a distance $b' = z_{RMS}^{PS}/2$ between two parallel planes.

In our experiment we find $z_{RMS}^{PS} \approx 126\,\text{nm}$ for the polystyrene microsphere and $z_{RMS}^{Au} \approx 110\,\text{nm}$ for the Au nanoparticle when we use l_c = 160 nm as the length of the DNA in the looped state. Since $R_B^{PS} \gg z_{RMS}^{PS}$ we may reasonably assume that the microsphere confines the DNA below itself much in the same way as the DNA is confined above the cover glass. An approximate way to calculate the hydrodynamic friction experienced by the DNA is to model this system as that of a spherical object diffusing between two planes, a problem that has been solved exactly in hydrodynamic theory[94,95]. The situation is somewhat complicated by the fact that the friction co- efficient is no longer isotropic, but has different in-plane and axial components, so we will consider each component separately.

To understand how hydrodynamic effects can lead to a two-fold increase in the friction on the DNA, and therefore change the lifetime of the loop accordingly, we com- pare the case of DNA diffusing or fluctuating near a single surface[96,97] to that of the same DNA diffusing between two surfaces (see Figure 6-3). These two cases are representative of the Au nanoparticle and polystyrene microsphere systems, respectively.

We first consider the case of surface tethered DNA attached to a Au nanoparticle. For this simple approximation we will treat the DNA as a sphere of effective radius *a*. The drag coefficient for the lateral motion of a sphere above a plane surface is approximated by Faxen's law[97].

$$\gamma_{\parallel} = \frac{\gamma_0}{1 - \frac{9}{16}x + \frac{1}{8}x^3 - \frac{45}{256}x^4 - \frac{1}{16}x^5}, \tag{6-13}$$

and an interpolation formula[96], to the same order, for the perpendicular drag coefficient is given by

$$\gamma_{\perp} = \frac{\gamma_0}{1 - \frac{9}{8}x + \frac{1}{2}x^3 - \frac{57}{100}x^4 + \frac{1}{5}x^5}, \tag{6-14}$$

In the above, $x = a/b$, where a is the effective radius of the DNA, b is the distance between the center of the DNA and the surface, and $\gamma_0 = 6\pi\eta a$ is the Stokes drag with viscosity η. Likewise, for the case of surface tethered DNA attached to a large microsphere, we must consider the parallel and perpendicular drag coefficients for the hydrodynamic motion of a sphere between two parallel surfaces, $\gamma_{\parallel}', \gamma_{\perp}'$. We do not have a simple interpolative formula for these coefficients, nonetheless, the values can be extracted from the numerical results reported by Ganatos *et al*. [94,95].

We next assume that the center of the DNA lies midway between the bead and the cover glass and we take this distance to be $b = z_{RMS}^{Au}/2$ and $b' = z_{RMS}^{PS}/2$, for the Au nanoparticles and the polystyrene microspheres respectively. If we assume that the effective radius of the DNA does not change, it follows that an effective radius for the DNA of $a = 0.57b'$ for in-plane motion and $a = 0.73b'$ for axial motion changes would lead to a friction coefficient of the DNA that is twice as large for the polystyrene microsphere experiment as for the Au nanoparticle experiment.

These values, which are similar in size, give reasonable estimates of 36-46nm for the effective hydrodynamic radius of the DNA segment responsible for loop breakdown. While this simple model does not prove that hydrodynamic effects on the diffusive behavior of the DNA give rise to the observed difference in looped lifetimes, the previous analysis does show that such effects are sufficiently large. Moreover, such hydrodynamic effects should have little effect on the protein due to its small size, which supports the

notion that fluctuations in the DNA, as opposed to the protein, are the primary cause for the breakdown of protein-mediated DNA loops. Unfortunately, it is difficult for us to directly assess the influence of such hydrodynamic forces as we postulate here; however, such forces could perhaps be better quantified through future microfluidic studies of polymer motion through a microchannel.

Chapter 7

Conclusions

We have quantitatively studied the effects of mechanical constraints and tension on the formation and breakdown of regulatory protein-DNA complexes using the constant-force axial optical tweezers. Since the high sensitivity of the protein-DNA complexes to mechanical tension has been theoretically predicted previously and then experimentally verified in our studies, it has become more than likely that there are mechanical pathways that regulate the expression of genes though DNA looping. The quantitative results that we have obtained can bring us one step closer to understanding the role of mechanics in gene regulation and other biological functions. In addition, the constant-force axial optical tweezers we developed is expected to become a powerful tool in biomechanical studies of protein-DNA interactions at the single-molecule level.

Chapter 2 shows that we have developed and characterized a new kind of optical tweezers setup, the constant-force axial optical tweezers, to manipulate submicron DNA molecules. Unlike conventional optical tweezers, which are usually limited to manipulating molecules that are longer than about a micron, the constant-force axial optical tweezers allows for accurate manipulation of submicron DNA molecules by pulling the microsphere attached at the end of the DNA away from the cover glass in the direction of the laser beam. In addition, by trapping the microsphere in the linear region of the optical

potential, where the optical force almost does not change with the axial position, the need for using a complex force-feedback control system to keep the optical force constant is eliminated, and the optical force can be simply adjusted by changing the laser intensity. When using this setup to measure protein-mediated DNA looping, since protein binding-induced DNA shortening can be measured directly from the axial position of the microsphere rather than from the Brownian motion of the microsphere, the temporal resolution of the measurement is about ten times better than that of conventional TPM. Moreover, by employing an autofocus feedback positioning system, the time of optical trapping is not limited by mechanical and thermal drifts.

In Chapter 3, the elasticity of submicron DNA molecules measured using the constant-force axial optical tweezers detailed in Chapter 2 is presented. By using this special optical tweezers, we are able to manipulate ds-DNA molecules that are as short as ~250 basepairs, which is almost an order of magnitude shorter than what can be studied with conventional optical tweezers. From the measurements of the force-extension curves of ds-DNA molecules ranging from 1298 to 247 bp in length, we show that the effective persistence length significantly decreases with a decreasing contour length. We attribute this observation to the entropic effects from the boundary conditions, which are large enough to significantly affect the available conformation space when the polymer is short. Because of the entropic boundary effects, the elasticity of a short entropic spring cannot be described by a simple intrinsic elasticity parameter analogous to Young's modulus, and the effective persistence length becomes boundary condition- and contour length-dependent, as demonstrated by our data. Our data show that, for example, the effective persistence length of the 247 bp-long DNA molecule is only about half of the value for

long DNA molecules. Moreover, we have shown that the excluded-volume force, which mainly results from the impenetrability of the cover glass, can stretch DNA molecules significantly when the molecules are short. Our results suggest that a boundary condition-dependent effective persistence length and the excluded-volume force should be taken into account when modeling DNA in a constrained environment or when interpreting experimental data in tethered-particle motion experiments with submicron DNA molecules.

Chapter 4 shows that, to study the effects of tension on the formation and breakdown of LacI-mediated DNA loops, we have used the constant-force axial optical tweezers to apply tension ranging from 60 to 183 fN to a DNA molecule that has two *lac* operators and measured the lifetimes of the looped and unlooped states. Our data show that the assembly of LacI-DNA complexes, which are crucial for regulating the expression of the *lac* genes, can be dramatically affected by miniscule forces on the order of a hundred femtonewtons. On the other hand, once formed, LacI-DNA complexes cannot be disrupted by tension in the substrate DNA easily. Considering that DNA *in vivo* is usually subject to piconewton forces, our results suggest the possibility of the existence of mechanical pathways that employ tension as a means of regulating the gene expression. In addition, we have used a simple polymer model and the measured force sensitivity of loop formation rate to determine the topology of LacI-mediated DNA loops and concluded that the antiparallel topology, which is more sensitive to force than the parallel topology, is the dominant topology of a generic LacI-mediated DNA loop.

Chapter 5 shows our measurements on the formation and breakdown of LacI-mediated DNA loops under an artificial fluctuating force applied by the optical tweezers to mimic fluctuations in a cellular environment. In contrast to the studies presented in

Chapter 4, the effects of fluctuations of different strengths on DNA looping are studied while the mean tension in the DNA molecule is kept constant. Our results show that the additional energy contributions from fluctuations, which are of only a little fraction of k_BT, can significantly increase the loop formation rate. However, once formed, the breakdown rate of DNA loops is unaffected by the applied fluctuations. The even more interesting result is that the sensitivity of the loop formation rate to the strength of the fluctuations is insensitive to the mean applied tension in the DNA. Our data suggest not only that noise from thermal and environmental fluctuations drives the loop formation, but that tension could be employed as a robust means of regulating transcription even in a noisy *in vivo* environment. Moreover, we have used a fluctuating barrier model, which is based on the measured sensitivity of the loop formation rate to static tension presented in Chapter 4, to explain our results and to predict the loop formation rates under different mean tension and fluctuations. This simple model is in excellent agreement with our experimental results.

Chapter 6 shows the effects of bead size on the formation and breakdown of protein-mediated DNA loops in TPM experiments. We have obtained data from both a conventional TPM experiment with 800 nm polystyrene microspheres and a darkfield TPM with 50 nm Au nanoparticles, and we have shown that the two loop formation rates are essentially the same and that the loop breakdown rate is extended less than two-fold by the presence of the large microsphere. These results are consistent with our expectation of weak excluded-volume effects and hydrodynamic surface interactions from the cover glass and the microsphere.

In short, we have conducted a series of quantitative studies to explore the mechanics of DNA and protein-mediated DNA looping in a constrained environment using the constant-force axial optical tweezers. We have gained quantitative insights into how static tension and fluctuations affect the loop formation and breakdown processes and how boundary conditions affect the effective persistence length of DNA.

In the future, to fully understand the role of mechanics in biological systems, it is needed to study the effects of other mechanical features, such as twist, supercoiling, DNA loop size, protein flexibility, operator alignment, sequence-dependent elasticity and intrinsic curvature, etc., on biological functions. In addition, it is important to develop *in vivo* fluorescence imaging techniques that can be used to observe protein-mediated DNA looping and other protein-DNA interactions so that single-molecule biomechanical studies can be conducted inside living cells directly. Moreover, to manipulate quantum dot- or Au nanoparticle-labeled DNA molecules inside living cells, other optical trapping techniques such as plasmonic trapping should be developed to trap these nanoparticles, which are small enough to enter cells, without generating much heat.

Appendix

The Operation Guide of the Constant-Force Axial Optical Tweezers

The calibration procedures for the constant-force axial optical tweezers and the method of measuring the optical potential have been detailed in Section 2.2.4 and 2.3.1 respectively. The procedures to position the attached microsphere in the linear region of the optical potential and to align the laser beam with the DNA molecule being measured in the xy plane are described here:

1. Roughly align the laser beam with the tethered microsphere in the xy plane. To be able to use the position feedback control system (detailed in Section 2.2.5) to compensate for drifts, there must be a microsphere that is stuck to the cover glass and is close to the tethered microsphere. However, the position feedback control system should not be turned on at this point.
2. Turn the laser beam (manipulation beam) on and off repeatedly using a custom LabVIEW program to control a data acquisition card to send a square-wave modulation signal to the Acousto-Optic Modulator (AOM). The laser beam is blocked when the voltage of the modulation signal is zero. When the laser beam is not blocked by the AOM, the intensity of the laser beam, which is proportional to the magnitude of the square wave, should be high enough to confine the Brownian motion of the tethered microsphere. On the other hand, to prevent the sample chamber from being heated up,

the intensity of the laser beam should not be too high, and the duration of each on-state should not be too long. Typical settings are about 300 ms for each on-state and about 600 ms for each off-state. The intensity of the laser was set at 250 mW, and the amplitude of the square wave was 0.5 V.

3. When the laser beam is turned on and off repeatedly, we can determine whether the laser beam is well aligned with the DNA molecule in the xy plane by observing the positions of the microsphere in images captured by the CCD. When the laser beam is not aligned with the DNA molecule, there is a preferred direction of motion when the modulation signal changes from zero to a positive value. For instance, if the microsphere moves more frequently to the right than to the left when the modulation signal changes from zero to a positive value, it means that the center of the optical trap is on the right of the DNA molecule. We can adjust the piezo-stage under the sample in the x direction until the microsphere moves equally frequently to the right and to the left. We can simply do it by eye. Similar adjustments need to be done in the y direction too. It should be noted that the alignment in the x and y directions might need to be done iteratively because when the sample is moved by the piezo-stage in one direction, sometimes there is a small unwanted movement in the other direction as well. The iterative alignment process needs to be continued until the microsphere moves equally frequently in all directions with respect to the center of the optical trap.
4. After the alignment in the xy plane, we move the sample stage in the z direction to roughly bring the tethered microsphere to the linear region of the optical potential, which is about 500 nm below the focal plane.

5. The laser beam is switched on and off repeatedly by the AOM again. A custom LabVIEW program that can determine the apparent size of the defocused image of the microsphere is used to measure the positions of the microsphere in the z direction while the DNA molecule is stretched repeatedly by the modulated laser beam. Since the midpoint of the linear region of the optical potential is the position where the optical force is strongest, to accurately position the tethered microsphere in the linear region, we can keep slightly adjusting the stage in the z direction until we find the position where the DNA extension is largest.
6. The alignment in the xy plane needs to be checked again because this might have changed when the z position was adjusted. If the laser beam is no longer well aligned with the DNA molecule, Step 2 to 5 should be repeated.
7. After the tethered microsphere is properly positioned in all dimensions, the CCD camera for the position feedback control system needs to be used to capture an image of the stuck microsphere. Then, NI Vision Assistant (National Instruments) is used to create a template for the geometric pattern matching based on the captured image.
8. The position feedback control system is turned on to compensate for thermal and mechanical drifts. The geometric pattern matching function in LabVIEW is used to find the center of each image of the microsphere by comparing each captured image with the image template created in Step 8. After turning on the position feedback control system, repeat Step 5 to make sure the microsphere is still in the linear region of the optical potential. If it is necessary to adjust the z position of the microsphere again, the position feedback control system needs to be turned off before the adjustment and to be turned on again after the adjustment.

Bibliography

1. Zimmerman, S. B. & Trach, S. O. Estimation of Macromolecule Concentrations and Excluded Volume Effects for the Cytoplasm of Escherichia-Coli. *J. Mol. Biol.* **222**, 599-620 (1991).

2. Ellis, R. J. Macromolecular crowding: obvious but underappreciated. *Trends Biochem. Sci.* **26**, 597-604 (2001).

3. Ralston, G. B. Effects of Crowding in Protein Solutions. *J. Chem. Educ.* **67**, 857-860 (1990).

4. Minton, A. P. Influence of excluded volume upon macromolecular structure and associations in 'crowded' media. *Curr. Opin. Biotechnol.* **8**, 65-69 (1997).

5. Bensimon, D. Force: A new structural control parameter? *Structure* **4**, 885-889 (1996).

6. Yin, H. *et al.* Transcription against an applied force. *Science* **270**, 1653-1657 (1995).

7. Brower-Toland, B. D. *et al.* Mechanical disruption of individual nucleosomes reveals a reversible multistage release of DNA. *Proc. Natl. Acad. Sci. USA* **99**, 1960-1965 (2002).

8. Hegner, M., Smith, S. B. & Bustamante, C. Polymerization and mechanical properties of single RecA-DNA filaments. *Proc. Natl. Acad. Sci. USA* **96**, 10109-10114 (1999).

9. Gemmen, G. J., Millin, R. & Smith, D. E. Tension-dependent DNA cleavage by restriction endonucleases: two-site enzymes are "switched off" at low force. *Proc. Natl. Acad. Sci. USA* **103**, 11555-11560 (2006).

10. Normanno, D., Vanzi, F. & Pavone, F. S. Single-molecule manipulation reveals supercoiling-dependent modulation of lac repressor-mediated DNA looping. *Nucleic Acids Res.* **36**, 2505-2513 (2008).

11. Jacob, F. & Monod, J. Genetic regulatory mechanisms in the synthesis of proteins. *J. Mol. Biol.* **3**, 318-356 (1961).

12. Matthews, K. S. DNA looping. *Microbiol. Rev.* **56**, 123-136 (1992).

13. Finzi, L. & Gelles, J. Measurement of lactose repressor-mediated loop formation and breakdown in single DNA-molecules. *Science* **267**, 378-380 (1995).

14. Blumberg, S., Gajraj, A., Pennington, M. W. & Meiners, J.-C. Three-dimensional characterization of tethered microspheres by total internal reflection fluorescence microscopy. *Biophys. J.* **89**, 1272-1281 (2005).

15. Lewis, M. The lac repressor. *C. R. Biol.* **328**, 521-548 (2005).

16. Oehler, S., Eismann, E. R., Krämer, H. & Müller-Hill, B. The three operators of the lac operon cooperate in repression. *EMBO J.* **9**, 973-980 (1990).

17. Schleif, R. DNA looping. *Annu. Rev. Biochem.* **61**, 199-223 (1992).

18. Rippe, K., Vonhippel, P. H. & Langowski, J. Action at a distance - DNA-looping and initiation of transcription. *Trends Biochem. Sci.* **20**, 500-506 (1995).

19. Dunn, T. M., Hahn, S., Ogden, S. & Schleif, R. F. An operator at -280 base pairs that is required for repression of araBAD operon promoter: addition of DNA helical turns between the operator and promoter cyclically hinders repression. *Proc. Natl. Acad. Sci. USA* **81**, 5017-5020 (1984).

20. Ptashne, M. & Gann, A. *Genes & signals*. (Cold Spring Harbor Laboratory Press, 2002).

21. Whitson, P. A., Olson, J. S. & Matthews, K. S. Thermodynamic analysis of the lactose repressor operator DNA interaction. *Biochemistry* **25**, 3852-3858 (1986).

22. Royer, C. A., Chakerian, A. E. & Matthews, K. S. Macromolecular binding equilibria in the lac repressor system: studies using high-pressure fluorescence spectroscopy. *Biochemistry* **29**, 4959-4966 (1990).

23. Levandoski, M. M. *et al.* Cooperative and anticooperative effects in binding of the first and second plasmid O^{sym} operators to a LacI tetramer: evidence for contributions of non-operator DNA binding by wrapping and looping. *J. Mol. Biol.* **260**, 697-717 (1996).

24. Lewis, M. *et al.* Crystal structure of the lactose operon repressor and its complexes with DNA and inducer. *Science* **271**, 1247-1254 (1996).

25. Villa, E., Balaeff, A. & Schulten, K. Structural dynamics of the lac repressor-DNA complex revealed by a multiscale simulation. *Proc. Natl. Acad. Sci. USA* **102**, 6783-6788 (2005).

26. Swigon, D., Coleman, B. D. & Olson, W. K. Modeling the Lac repressor-operator assembly: the influence of DNA looping on Lac repressor conformation. *Proc. Natl. Acad. Sci. USA* **103**, 9879-9884 (2006).

27. Balaeff, A., Mahadevan, L. & Schulten, K. Modeling DNA loops using the theory of elasticity. *Phys. Rev. E* **73** (2006).

28. Goyal, S. *et al.* Intrinsic Curvature of DNA Influences Lac-R Mediated Looping. *Biophys. J.* **93**, 4342-4359 (2007).

29. Vanzi, F., Broggio, C., Sacconi, L. & Pavone, F. S. Lac repressor hinge flexibility and DNA looping: single molecule kinetics by tethered particle motion. *Nucleic Acids Res.* **34**, 3409-3420 (2006).

30. Wong, O. K., Guthold, M., Erie, D. A. & Gelles, J. Interconvertible lac repressor-DNA loops revealed by single-molecule experiments. *PLoS Biol.* **6**, e232 (2008).

31. Chen, Y.-F., Milstein, J. N. & Meiners, J.-C. Femtonewton entropic forces can control the formation of protein-mediated DNA loops. *Phys. Rev. Lett.* **104**, 048301 (2010).

32. Smith, S. B., Finzi, L. & Bustamante, C. Direct mechanical measurements of the elasticity of single DNA molecules by using magnetic beads. *Science* **258**, 1122-1126 (1992).

33. Wang, M. D., Yin, H., Landick, R., Gelles, J. & Block, S. M. Stretching DNA with optical tweezers. *Biophys. J.* **72**, 1335-1346 (1997).

34.Marko, J. F. & Siggia, E. D. Driving proteins off DNA using applied tension. *Biophys. J.* **73**, 2173-2178 (1997).

35. Blumberg, S., Tkachenko, A. V. & Meiners, J.-C. Disruption of protein-mediated DNA looping by tension in the substrate DNA. *Biophys. J.* **88**, 1692-1701 (2005).

36. Blumberg, S., Pennington, M. W. & Meiners, J.-C. Do femtonewton forces affect genetic function? A review. *J. Biol. Phys.* **32**, 73-95 (2006).

37. Ashkin, A. Acceleration and trapping of particles by radiation pressure. *Phys. Rev. Lett.* **24**, 156-159 (1970).

38.Ashkin, A. & Dziedzic, J. M. Optical levitation by radiation pressure. *Appl. Phys. Lett.* **19**, 283-285 (1971).

39. Ashkin, A., Dziedzic, J. M., Bjorkholm, J. E. & Chu, S. Observation of a single-beam gradient force optical trap for dielectric particles. *Opt. Lett.* **11**, 288-290 (1986).

40. Meiners, J.-C. & Quake, S. R. Femtonewton force spectroscopy of single extended DNA molecules. *Phys. Rev. Lett.* **84**, 5014 (2000).

41.Revyakin, A., Ebright, R. H. & Strick, T. R. Single-molecule DNA nanomanipulation: improved resolution through use of shorter DNA fragments. *Nat. Methods* **2**, 127-138 (2005).

42. Wang, M. D. *et al.* Force and velocity measured for single molecules of RNA polymerase. *Science* **282**, 902-907 (1998).

43. Smith, D. E. *et al.* The bacteriophage ϕ29 portal motor can package DNA against a large internal force. *Nature* **413**, 748-752 (2001).

44. Liesfeld, B., Nambiar, R. & Meiners, J.-C. Particle transport in asymmetric scanning-line optical tweezers. *Phys. Rev. E* **68**, 051907 (2003).

45. Nambiar, R., Gajraj, A. & Meiners, J.-C. All-optical constant-force laser tweezers. *Biophys. J.* **87**, 1972-1980 (2004).

46. Greenleaf, W. J., Woodside, M. T., Abbondanzieri, E. A. & Block, S. M. Passive all-optical force clamp for high-resolution laser trapping. *Phys. Rev. Lett.* **95** (2005).

47. Abbondanzieri, E. A., Greenleaf, W. J., Shaevitz, J. W., Landick, R. & Block, S. M. Direct observation of base-pair stepping by RNA polymerase. *Nature* **438**, 460-465 (2005).

48. Meiners, J.-C. & Quake, S. R. Direct measurement of hydrodynamic cross correlations between two particles in an external potential. *Phys. Rev. Lett.* **82**, 2211 (1999).

49. Rohrbach, A. & Stelzer, E. H. K. Three-dimensional position detection of optically trapped dielectric particles. *J. Appl. Phys.* **91**, 5474-5488 (2002).

50. Deufel, C. & Wang, M. D. Detection of forces and displacements along the axial direction in an optical trap. *Biophys. J.* **90**, 657-667 (2006).

51. Hsieh, W. T., Whitson, P. A., Matthews, K. S. & Wells, R. D. Influence of sequence and distance between two operators on interaction with the lac repressor. *J. Biol. Chem.* **262**, 14583-14591 (1987).

52. Revyakin, A., Allemand, J. F., Croquette, V., Ebright, R. H. & Strick, T. R. Single-molecule DNA nanomanipulation: detection of promoter-unwinding events by RNA polymerase. *Methods Enzymol.* **370**, 577-598 (2003).

53. Viana, N. B., Freire, R. T. & Mesquita, O. N. Dynamic light scattering from an optically trapped microsphere. *Phys. Rev. E* **65**, 041921 (2002).

54. Rocha, M. S., Viana, N. B. & Mesquita, O. N. DNA-psoralen interaction: a single molecule experiment. *J. Chem. Phys.* **121**, 9679-9683 (2004).

55. Rohrbach, A. Switching and measuring a force of 25 femtoNewtons with an optical trap. *Opt. Express* **13**, 9695-9701 (2005).

56. Brenner, H. The slow motion of a sphere through a viscous fluid towards a plane surface. *Chem. Eng. Sci.* **16**, 242-251 (1961).

57. Neuman, K. C. & Block, S. M. Optical trapping. *Rev. Sci. Instrum.* **75**, 2787-2809 (2004).

58. Neuman, K. C., Abbondanzieri, E. A. & Block, S. M. Measurement of the effective focal shift in an optical trap. *Opt. Lett.* **30**, 1318-1320 (2005).

59. Gouesbet, G., Maheu, B. & Gréhan, G. Light scattering from a sphere arbitrarily located in a Gaussian beam, using a Bromwich formulation. *J. Opt. Soc. Am. A-Opt. Image Sci. Vis.* **5**, 1427-1443 (1988).

60. Harada, Y. & Asakura, T. Radiation forces on a dielectric sphere in the Rayleigh scattering regime. *Opt. Commun.* **124**, 529-541 (1996).

61. Nieminen, T. A. *et al.* Optical tweezers computational toolbox. *J. Opt. A-Pure Appl. Opt.* **9**, S196-S203 (2007).

62. Seol, Y., Li, J., Nelson, P. C., Perkins, T. T. & Betterton, M. D. Elasticity of short DNA molecules: theory and experiment for contour lengths of 0.6-7 μm. *Biophys. J.* **93**, 4360-4373 (2007).

63. Segall, D. E., Nelson, P. C. & Phillips, R. Volume-exclusion effects in tethered-particle experiments: bead size matters. *Phys. Rev. Lett.* **96**, 088306 (2006).

64. Marko, J. F. & Siggia, E. D. Stretching DNA. *Macromolecules* **28**, 8759-8770 (1995).

65. Bustamante, C., Marko, J. F., Siggia, E. D. & Smith, S. B. Entropic elasticity of λ-phage DNA. *Science* **265**, 1599-1600 (1994).

66. Bouchiat, C. *et al.* Estimating the persistence length of a worm-like chain molecule from force-extension measurements. *Biophys. J.* **76**, 409-413 (1999).

67. Bustamante, C., Bryant, Z. & Smith, S. B. Ten years of tension: single-molecule DNA mechanics. *Nature* **421**, 423-427 (2003).

68. Samuel, J. & Sinha, S. Elasticity of semiflexible polymers. *Phys. Rev. E* **66**, 050801 (R) (2002).

69. Pampaloni, F. *et al.* Thermal fluctuations of grafted microtubules provide evidence of a length-dependent persistence length. *Proc. Natl. Acad. Sci. USA* **103**, 10248-10253 (2006).

70. Cloutier, T. E. & Widom, J. DNA twisting flexibility and the formation of sharply looped protein-DNA complexes. *Proc. Natl. Acad. Sci. USA* **102**, 3645-3650 (2005).

71. Du, Q., Smith, C., Shiffeldrim, N., Vologodskaia, M. & Vologodskii, A. Cyclization of short DNA fragments and bending fluctuations of the double helix. *Proc. Natl. Acad. Sci. USA* **102**, 5397-5402 (2005).

72. Tkachenko, A. V. arXiv:q-bio/0703026v1 [q-bio.BM].

73. Pouget, N. *et al.* Single-particle tracking for DNA tether length monitoring. *Nucleic Acids Res.* **32**, e37 (2004).

74. Qian, H. & Elson, E. L. Quantitative study of polymer conformation and dynamics by single-particle tracking. *Biophys. J.* **76**, 1598-1605 (1999).

75. Chen, Y.-F., Blab, G. A. & Meiners, J.-C. Stretching submicron biomolecules with constant-force axial optical tweezers. *Biophys. J.* **96**, 4701-4708 (2009).

76. Wilson, C. J., Zhan, H., Swint-Kruse, L. & Matthews, K. S. The lactose repressor system: paradigms for regulation, allosteric behavior and protein folding. *Cell. Mol. Life Sci.* **64**, 3-16 (2007).

77. Vilar, J. M. G. & Leibler, S. DNA looping and physical constraints on transcription regulation. *J. Mol. Biol.* **331**, 981-989 (2003).

78. Han, L. *et al.* Concentration and length dependence of DNA looping in transcriptional regulation. *PLoS ONE* **4**, e5621 (2009).

79. Yan, J., Kawamura, R. & Marko, J. F. Statistics of loop formation along double helix DNAs. *Phys. Rev. E* **71**, 061905 (2005).

80. Towles, K. B., Beausang, J. F., Garcia, H. G., Phillips, R. & Nelson, P. C. First-principles calculation of DNA looping in tethered particle experiments. *Phys. Biol.* **6**, 025001 (2009).

81. Chen, Y.-F., Wilson, D. P., Raghunathan, K. & Meiners, J.-C. Entropic boundary effects on the elasticity of short DNA molecules. *Phys. Rev. E* **80**, 020903(R) (2009).

82. Frank, D. E. *et al.* Thermodynamics of the interactions of Lac repressor with variants of the symmetric Lac operator: effects of converting a consensus site to a non-specific site. *J. Mol. Biol.* **267**, 1186-1206 (1997).

83. Maniotis, A. J., Chen, C. S. & Ingber, D. E. Demonstration of mechanical connections between integrins cytoskeletal filaments, and nucleoplasm that stabilize nuclear structure. *Proc. Natl. Acad. Sci. USA* **94**, 849-854 (1997).

84. Ellis, R. J. & Minton, A. P. Join the crowd. *Nature* **425**, 27-28 (2003).

85. Rivas, G., Ferrone, F. & Herzfeld, J. Life in a crowded world. *EMBO Rep.* **5**, 23-27 (2004).

86. Mizuno, D., Tardin, C., Schmidt, C. F. & MacKintosh, F. C. Nonequilibrium mechanics of active cytoskeletal networks. *Science* **315**, 370-373 (2007).

87. Liverpool, T. B. Active gels: where polymer physics meets cytoskeletal dynamics. *Philos. Trans. R. Soc. A-Math. Phys. Eng. Sci.* **364**, 3335-3355 (2006).

88. Ilg, P. & Barrat, J. L. Driven activation vs. thermal activation. *EPL* **79**, 26001 (2007).

89. Gallet, F., Arcizet, D., Bohec, P. & Richert, A. Power spectrum of out-of-equilibrium forces in living cells: amplitude and frequency dependence. *Soft Matter* **5**, 2947-2953 (2009).

90. Gota, C., Okabe, K., Funatsu, T., Harada, Y. & Uchiyama, S. Hydrophilic fluorescent nanogel thermometer for intracellular thermometry. *J. Am. Chem. Soc.* **131**, 2766-2767 (2009).

91. Gardiner, C. W. *Handbook of stochastic methods for physics, chemistry, and the natural sciences*. 3rd edn, (Springer-Verlag, 2004).

92. Nelson, P. C. Colloidal particle motion as a diagnostic of DNA conformational transitions. *Current Opinion in Colloid & Interface Science* **12**, 307-313 (2007).

93. Thompson, R., Larson, D. & Webb, W. Precise nanometer localization analysis for individual fluorescent probes. *Biophys. J.* **82**, 2775-2783 (2002).

94. Ganatos, P., Weinbaum, S. & Pfeffer, R. A strong interaction theory for the creeping motion of a sphere between plane parallel boundaries. Part 1. Perpendicular Motion. *J. Fluid Mech.* **99**, 739-753 (1980).

95. Ganatos, P., Pfeffer, R. & Weinbaum, S. A strong interaction theory for the creeping motion of a sphere between plane parallel boundaries. Part 2. Parallel motion. *J. Fluid Mech.* **99**, 755-783 (1980).

96. Schaffer, E., Norrelykke, S. F. & Howard, J. Surface forces and drag coefficients of microspheres near a plane surface measured with optical tweezers. *Langmuir* **23**, 3654-3665 (2007).

97. Happel, J. & Brenner, H. *Low Reynolds number hydrodynamics. With special applications to particulate media*. 1st edn, (Noordhoff International Publishing, 1983).